NASA Technical Paper 1421

Wind-Tunnel Investigation of the Validity of a Sonic-Boom-Minimization Concept

Robert J. Mack and Christine M. Darden

OCTOBER 1979

NASA

Wind-Tunnel Investigation of the Validity of a Sonic-Boom-Minimization Concept

Robert J. Mack and Christine M. Darden
Langley Research Center
Hampton, Virginia

SUMMARY

A wind-tunnel investigation has been conducted to determine the validity and applicability of a sonic-boom-minimization theory. Five models – two reference and three low-boom constrained – were tested at design Mach numbers of 1.5 and 2.7 and at angles of attack which provided the same lift. Pressure signatures were measured at a distance of 3 low-boom body lengths and were compared with signatures computed from descriptions of model geometry. Sensitivity studies were performed on the low-boom models at angles of attack 20 percent above and below the design point at Mach numbers of 1.5, 2.6, 2.7, and 2.8.

Results showed that the pressure signatures generated by the low-boom models had significantly lower overpressure levels than those produced by the reference models. Mach number and angle-of-attack sensitivity of the low-boom-model pressure signatures were found to be small.

Boundary-layer effects were sizable on the low-boom models, and when viscous corrections were included in the analysis, improved agreement between the predicted and the measured signatures was noted. However, the agreement was better at Mach 1.5 than at Mach 2.7. It was concluded that the minimization theory was valid at Mach 1.5 and was probably valid at Mach 2.7, with further study needed to resolve the uncertainty.

INTRODUCTION

The first supersonic cruise aircraft were designed to fly at the highest possible aerodynamic efficiency with little concern given to the sonic boom these aircraft would generate. However, ground overpressures from aircraft in test flights at supersonic Mach numbers were found to be so high as to cause considerable public concern. As a result, legal prohibitions on the overland supersonic flight of commercial transports were passed. Clearly, low sonic boom would have to be an equally important consideration along with other factors in the design of future supersonic transport aircraft for there to be any hope of removing present restrictions.

An analytic method that would permit sonic-boom minimizing constraints to directly influence the overall aircraft design was derived by Seebass and George (ref. 1). The method provides a constraint on the aircraft equivalent-area distribution. Aircraft features can be shaped and components positioned within this area envelope so as to keep the ground overpressures at a predetermined level while maximum aerodynamic and structural efficiencies are being sought. A previous analytical study (ref. 2) showed that sonic-boom levels could be reduced considerably by judiciously applying these boom-minimization concepts. These favorable results indicated the need for experimental verification of the minimization method by a wind-tunnel test program involving models designed to match sonic-boom constraints.

Five wing-body models were used in this wind-tunnel study. There were two reference models - an unconstrained delta wing and an unconstrained arrow wing - and three models designed for low-boom performance - one Mach 1.5 low-boom arrow-wing and two Mach 2.7 low-boom arrow-wing models. The nonboom-constrained models were included to provide reference pressure signatures that could be compared with those produced by the minimum sonic-boom models.

Pressure signatures were measured at a distance of 45.72 cm (18.0 in.), which is 3 low-boom body lengths. Design Mach numbers were 1.5 and 2.7; additional tests were performed at Mach numbers of 2.6 and 2.8 and at angle-of-attack to design-angle-of-attack ratios of 0.8, 1.0, and 1.2 to determine the shape and overpressure sensitivity of the low-boom pressure signatures.

SYMBOLS

Because these wind-tunnel models were designed initially as full-size aircraft (with enlargements for sting support), certain parameters such as l_e, A_e, and x_e, have two characteristic sets of dimensions. When the full-scale aircraft is referred to, the dimensions are in meters (feet); when the model is referred to, the dimensions are in centimeters (inches).

A_e	effective area due to area-ruled volume and lift
C_{L_α}	theoretical lift-curve slope
D	model sting diameter
d	dihedral height
F	Whitham F-function
h	radial distance normal to wind vector from nose (see fig. 10)
Δh	incremental displacement of model nose due to lift (see fig. 9(a))
K_r	sonic-boom reflection factor
k	deflection per unit load of model nose, $\Delta\alpha/\Delta L$
ΔL	incremental lift load used to determine k (see fig. 9(b))
l	overall length of model or aircraft
l_e	effective length of model or aircraft
M	free-stream Mach number
p	free-stream static pressure, Pa (lbf/ft^2)

2

Δp incremental pressure due to model flow field, Pa (lbf/ft^2)

q wind-tunnel dynamic pressure, $\dfrac{\gamma}{2} pM^2$, Pa (lbf/ft^2)

S wing area

W_c aircraft weight at start of cruise, kg (lb)

x longitudinal ordinate

Δx incremental distance along pressure signature

x_e effective distance along windward direction

y spanwise coordinate

α angle of attack, degrees and minutes

$\Delta\alpha$ change in α due to lift-induced sting deflection (see fig. 9)

β $= \sqrt{M^2 - 1}$

γ ratio of specific heats (1.4 for air)

δ_e^* effective area due to estimated boundary-layer displacement thickness

ϵ wind-tunnel flow angle along model travel, arc minutes

θ angle setting on prism in angle-of-attack mechanism, degrees and minutes

λ fraction of equivalent length for nose "spike" (see fig. 5)

μ Mach angle, $\sin^{-1}\dfrac{1}{M}$

Subscripts:

D design condition at cruise Mach number and altitude

f fuselage

le leading edge

w wing

Current minimum-boom theory and design methods are due to the accumulated efforts of many researchers during the past quarter century. The basic sonic-boom theory originated in a classic paper (ref. 3) by G. B. Whitham. Whitham theory is a modification of linearized theory to account for the coalescense of disturbances into shocks for bodies of revolution. Basic to its application is the formulation of the F-function which relates the area distribution of the aircraft that is generating flow-field disturbances to an appropriate source distribution. The analysis of reference 4 showed that Whitham theory could also be applied to winged bodies. Since efficient supersonic cruise aircraft are, in general, slender small-disturbance bodies, Whitham theory has been useful in predicting sonic-boom overpressures.

Concurrently with theory-validating experimental programs such as those mentioned in reference 5, studies were conducted to define minimum-sonic-boom-generating bodies. The concept of the far-field lower bound was introduced in reference 6. For these lower-bound bodies, F-functions are simply delta-function pulses which give effective areas A_e proportional to $x_e^{1/2}$ (fig. 1) and which generate minimum-impulse, far-field, N-wave signatures. Aircraft represented by lower-bound effective areas are usually very blunt and have high drag characteristics.

A later analysis, reference 7, pointed out that because of the appreciable length of proposed supersonic cruise aircraft, near-field characteristics of the pressure signature could persist out to significant distances at Mach numbers up to $\sqrt{2}$. An experimental study which tested these concepts is described in reference 8. The good agreement between measured and predicted pressure signatures at $M = 2.0$ as well as $M = \sqrt{2}$ proved that the basic idea was sound.

Further progress in the development of sonic-boom theory came from the signature-propagation work of reference 9. In a report which described a computer program for extrapolating a pressure signature through a stratified atmosphere, it was shown that real atmosphere effects tended to "freeze" the signature shape well before the pressure disturbances reached the ground. This reinforced the earlier hypothesis that near-field shape features would be preserved during the transonic acceleration phase of flight and extended it to supersonic cruise conditions.

The far-field minimum-boom concept, the shape-persistence hypothesis, and the shape-freezing tendencies of the atmosphere were combined into the isothermal-atmosphere-boom-minimization theory of reference 1. A delta-function pulse was placed at the front of a flat-top F-function or at the front of a linearly increasing F-function in a manner that minimized the shock overpressure or the nose shock, respectively. Also, a provision for making the tail shock equal in strength to the nose shock was included. The work of references 10 and 11 extended the minimization theory of reference 1 to a standard atmosphere and replaced the delta-function pulse with a finite, triangular "spike." It was shown that this modification would produce a configuration with a lower drag and only a small increase in shock overpressure and impulse. In figure 1, a comparison of effective-area distributions computed from the minimum-impulse F-function of reference 6, the minimum-overpressure F-function

4

of reference 1, and the spiked F-function of reference 11 is shown to illustrate the development of minimization concepts. Only the positive part of the F-function, where the effects of the different area constraints are most evident, is shown in each case. Overpressures for each body, calculated at a typical cruise altitude, are also shown.

The curves are calculated for bodies of length l_e and a maximum effective area of $0.01 l_e^2$. A peak-to-plateau ratio on the spiked F-function was 6.5, about the same value as on the F-functions of the models designed for minimum boom at $M = 2.7$. The flat-top F-function of reference 1 was calculated from the same propagation condition that was imposed on the spiked F-function; that is, on the ground the pulse and the "spike" would disappear.

The far-field, minimum-impulse F-function of reference 6 gives a high-drag body because of the rapid growth of equivalent area. Some drag reduction is possible on the body designed from the F-function of reference 1 along with a substantial reduction in overpressure. Further drag reductions are possible on the body which gives the spiked F-function of reference 11, but at the penalty of slightly higher overpressures than from the signature of reference 1. Since the spike width is variable, drag—sonic-boom trade-off studies are possible. In the present wind-tunnel study, $\lambda = 0.1$ was used in the calculation of minimum-boom-constraint curves for the low-boom models.

MODEL DESCRIPTION

The five models used in the study are shown in figure 2, where their plan-view features and relative size can be easily seen. Two models - the delta wing and the arrow wing - were the reference models, while the other three were designed to low-boom constraints. They are 1/600-scale copies of full-size aircraft. Inviscid-flow assumptions were used in designing the low-boom models to meet equivalent-area constraints. However, Reynolds numbers effects were included in the analysis of data by adding an incremental effective area due to displacement thickness which was computed from the method of reference 12.

Since basic sonic-boom minimization concepts were being tested, wing-body models were judged sufficient to demonstrate the effects of the volume and lift contributions. Aircraft components such as horizontal and vertical tails, engine nacelles, and wing fences were not included to simplify design and construction. For the same reasons, the models were designed with circular, uncambered fuselages and flat, planar wings having sharp leading and trailing edges.

Reference Models

An unconstrained delta-wing model which resembled an early supersonic cruise vehicle concept and an unconstrained arrow-wing model with features that emphasized high-aerodynamic-efficiency, supersonic cruise technology were used as standards for comparison of performance with the three models configured for low sonic boom. A three-view drawing of the delta-wing-body model is seen in figure 3(a) and that of the arrow-wing-body model in figure 3(b).

5

Low-Boom Models

The three low-boom models were obtained by designing aircraft according to the minimum sonic-boom area distributions obtained from the computer program of reference 11. Two aircraft were designed to cruise at M = 2.7 and an altitude of 18 288 m (60 000 ft) while the third was to cruise at M = 1.5 and an altitude of 15 240 m (50 000 ft). A Mach number of 2.7 was chosen because it was used in the early feasibility studies and is approaching the upper limits of near-field sonic-boom theory. A Mach number of 1.5 was judged to be near the lower limit for a supersonic cruise aircraft and is in the range where linearized theory is accepted as valid for slender bodies.

A schematic outline of the computerized sonic-boom minimization process which calculates the effective-area constraint curve, the F-function, and the ground pressure signature is shown in figure 4. The input parameters are listed as design conditions. Note that neither the minimum nose shock Δp nor the minimum overpressure Δp is among the input parameters. These pressures are a function of the design conditions and must be assessed by the designer as either excessive or satisfactory. If Δp is too large, one or more design conditions must be changed and the program recycled until an acceptable value is calculated.

For all three of the test low-boom models, the minimum overpressure (spiked, flat-top) option was chosen with an acceptable Δp from their full-scale counterpart to be approximately 50 Pa (1 lbf/ft^2). The ratio of nose to tail shock of the pressure signatures was 1.0.

Although the minimization procedure provides an effective-area curve, the aircraft meeting this constraint can still reflect a variety of design approaches. This is illustrated in figure 5 for two Mach 2.7 low-boom wing-body configurations. Both aircraft meet the same design conditions, have the same "spike" flat-top F-function, and produce the same ground-level sonic-boom signature. The most noticeable differences are in the wing planforms and the effective-area distributions of the volume and the lift. Obviously there is no unique aircraft shape. Other configurations can be designed to meet the same cruise flight conditions and still produce the same minimum overpressure signature. This is due to the variety of ways that lift and volume can be combined to satisfy both sonic-boom constraints and aerodynamic, structural, etc. requirements.

The three low-boom aircraft were designed with a cruise weight of 272 155 kg (600 000 lb) and an equivalent length of 91.44 m (300 ft). In addition, the "spike" width ratio λ was chosen as 0.1, since this represented a first-cut trade-off between shock level and drag. This is the only drag consideration included in the study. A ground-reflection factor of 1.9 was used in the pressure-signature calculations.

Additional effective area was included to account for the effects of the model sting, which was sized to withstand the stresses to be imposed. Its effective area was then included in the minimization program so that the final effective-area constraint curve included sting effects.

6

Two aircraft were designed to match the minimum overpressure-equivalent-area curve defined from a Mach number of 2.7 and an altitude of 18 288 m (60 000 ft), and one aircraft was designed to match the constraint curve defined from a Mach number of 1.5 and an altitude of 15 240 m (50 000 ft). Of the two aircraft designed for M = 2.7, one used only volume to meet area requirements near the nose while the other - a blunt-apex arrow - used both volume and lift. Figures 2 and 5 illustrate the differences between these two Mach 2.7 aircraft.

The design process was iterative and began by making a first-cut wing-body design. This design was analyzed with the wave-drag area rule program (ref. 13) and a wing analysis program (ref. 14) which had been modified to calculate both volume and lift effective-area contributions. A comparison of the resulting equivalent-area curve and the constraint curve indicated where changes should be made to improve the agreement of the curves. This iteration process was continued until acceptable agreement was reached.

The features common to all the final designs are shown in figure 6 and were varied in the iteration process to match the effective areas. Wing camber and twist were not employed because of the small size of the models, but dihedral was used specifically to control effective length. The effect of dihedral on the effective length is shown in figure 7.

When a satisfactory solution was obtained, 1/600-scale wind-tunnel models were constructed from the designs. Three-view drawings of these designs are shown in figures 8(a), 8(b), and 8(c). Detailed descriptions (in wave-drag program format) of the full-size aircraft are given in table I.

TEST APPARATUS AND PROCEDURE

Model Deflection Measurements

Since the models were 1/600 scale (i.e., 15.24 cm (6.0 in.) or less in length), a small prism for measuring the model angle of attack was mounted in the sting support of the angle-of-attack mechanism. Attitude and position corrections were obtained from a measurement of model deflection and pitch-angle increments due to imposed static loads. Figure 9(a) shows a sketch of the undeflected and deflected model; figure 9(b), the deflection lines obtained with the models under load in the angle-of-attack mechanism. These lines were computed from a linear, least-squares fit of the measurement points. Note that corrections in both angle and displacement were recorded, the first for determining the correct prism angle and the second as an incremental correction to the distance between model and measuring probe.

Pressure-Measurement Apparatus

Figure 10 is a sketch of the model, model support system, and pressure rake used during the test. Model angle of attack is controlled by the angle-of-attack mechanism mounted on the model longitudinal motion actuator. Angle of attack is positive in rotation away from the pressure rake and is measured

with a wind-tunnel spectrometer from the prism set into the model sting-support arm of the angle-of-attack mechanism (fig. 9(a)).

The model is moved forward or aft during the measurement of the pressure signature by the model longitudinal actuator mounted on the wind-tunnel side-wall. Differential pressures were measured with a pressure rake having a measuring probe and a reference probe mounted in the offset position shown in figure 10. Each probe was a 2° half-angle cone with two orifices set 180° apart connected to a common chamber. The measuring probe was positioned in a plane which coincided with the model plane of symmetry in pitch. Its axis was parallel with the tunnel center line and the orifices were positioned 90° to the plane containing the probe axis and the model plane of symmetry.

The pressure probes and rake were mounted on the tunnel sting support, which provided positioning both longitudinally along the tunnel test section as well as laterally across the test section (i.e., toward and away from the model). Model and measuring probe positioning were remotely controlled during the test run from the control console.

Pressure Measurements

The wind-tunnel tests were conducted at a Mach number of 1.5 in the low-speed test section and at Mach numbers of 2.6, 2.7, and 2.8 in the high-speed test section of the Langley Unitary Plan wind tunnel. Constant values of Reynolds number, 6.56×10^6 per meter (2.0×10^6 per foot), and stagnation temperature, 338.7 K (150° F), were maintained at all Mach numbers. The stagnation pressures used were 53 195 Pa (1111 lb/ft^2), 85 675 Pa (1790 lb/ft^2), 90 397 Pa (1888 lb/ft^2), and 95 329 Pa (1991 lb/ft^2) at Mach numbers of 1.5, 2.6, 2.7, and 2.8, respectively.

Flow-angle surveys established incremental flow angles of 6.8 arc minutes and 6.0 arc minutes (angled away from the tunnel sidewall) for the respective Mach numbers of 1.5 and 2.7. Surveys were not made at Mach numbers of 2.6 and 2.8 because it was assumed that the ±0.1 increment in Mach number would not change the flow angle significantly. These flow-angle increments were used to correct the prism-angle settings so that the models would be at the required angle of attack. (See fig. 9(a).)

Pressure signatures were measured at a distance (normal to the wind direction) of 45.72 cm (18 in.) from the model nose. The individual pressure signatures produced by the reference models and the Mach 2.7 low-boom arrow-wing models are shown in figures 11(a) to 11(d). In figures 11(e) and 11(f), these signatures have been overlaid to facilitate comparisons between the reference models and the two low-boom models. A similar arrangement of measured pressure signatures is seen in figures 12(a) to 12(d) for the reference models and the Mach 1.5 low-boom arrow-wing model. In both figures 11 and 12, the angles of attack are those calculated to produce a level-flight lift of 272 155 kg (600 000 lb) on the full-scale aircraft.

For the Mach 2.7 low-boom models, sensitivity studies were made for both angle of attack and Mach number. Sensitivity to angle of attack was investi-

8

gated at Mach numbers of 1.5 and 2.7 by measuring pressure signatures at angles which were 20 percent above and below the design angle of attack. (See table II.) Mach number sensitivity pressure signatures were measured at Mach numbers of 2.6 and 2.8 with the Mach 2.7 low-boom arrow-wing model set at design-lift angle of attack. Since stable supersonic flow could not be established at a Mach number of 1.4, the Mach number sensitivity tests were not made for the Mach 1.5 low-boom model.

In figures 13(a) and 13(b), the results of these angle-of-attack and Mach number sensitivity tests are shown for the Mach 2.7 low-boom arrow-wing model. Since the measured pressure signatures from the angle-of-attack sensitivity tests for the Mach 1.5 low-boom arrow-wing model and the Mach 2.7 low-boom, blunt-apex arrow-wing model showed the same trends, they were not included in this report.

RESULTS AND DISCUSSION

The measured pressure signatures of figures 11 to 13 show distinct differences which mark them as generated by either the reference models or by the low-boom models. In figure 11(a), the effects of rapid lift buildup and short lift development length are seen as a near-field N-wave. Figure 11(b) shows that a more gradual lift buildup coupled with a slightly longer lift development length gives a pressure signature in which both the nose and the lift-induced shocks are seen in the near field. Similar results were measured at $M = 1.5$ also, as seen in figures 12(a) and 12(b).

In contrast, the pressure signatures from the low-boom models (figs. 11(c), 11(d), and 12(c)) show the benefits of a gradual and constrained lift buildup, an appreciably extended lift development length, special nose blunting, etc. Definite near-field and flat-top characteristics are seen, although they are somewhat masked by unexpected ripples and overshadowed by a compression peak just before the final expansion. As will be shown, a significant amount of these departures from the desired pressure signatures can be attributed to sizable viscous effects on the small wind-tunnel models. These effects were not included in the full-scale aircraft designs because they could not be properly scaled down to model size.

Signatures from the unconstrained models and each of the low-boom models are overlaid for easier comparisons in figures 11(e), 11(f), and 12(d). Considering only the forward part of the low-boom signatures, where viscous effects are small, these comparisons show the low-boom pressure levels to be about one-third those of the delta wing and about one-half those of the arrow wing – a significant reduction.

The relative sensitivity of signature shape and overpressure strength to off-design Mach number and angle of attack is seen in figure 13. A change of ±0.1 in Mach number is barely noticeable on the pressure signatures in figure 13(a). The prominent differences between the three signatures in figure 13(b) reflect a 20-percent change in angle of attack. If the angle-of-attack increments were of the same proportionate size as the Mach number increments, very little difference in shape or overpressure strength would be

seen. These results indicate that shock strength and impulse levels in minimum-overpressure signatures are relatively insensitive to changes of 3 to 4 percent in Mach number and/or angle of attack.

In order to estimate the viscous effects on the wind-tunnel models, boundary-layer displacement thicknesses on the wing and body surfaces were calculated using the method of reference 12, and the incremental area contributions were added to the distributions of model effective area due to volume. These displacement-thickness-modified areas were used along with the original lift distributions to get a new set of corrected theoretical signatures.

In figures 14(a) to 14(c), effective-area distributions, a measured pressure signature, and three theoretical pressure signatures are shown and compared for each of the low-boom models at their respective design condition. The inviscid-theory signatures were calculated from the measurements of the constructed models; the theory (with viscous effects) signatures were calculated from the model measurements plus corrections for boundary-layer displacement thickness; and the inviscid, boom-constrained theory signatures were calculated from the low-boom F-function provided by the minimization program of reference 11.

These signature comparisons were made at a distance of 3 body lengths rather than at an extrapolated ground distance because the model boundary layer was not the same as, or necessarily similar to, the boundary layer on the full-scale aircraft. A discussion of signature extrapolation is presented after the comparison of signatures.

Since both the measured and the predicted signatures are near-field, some of the F-function "spike" is still seen at, and just aft of, the nose shock. This residual minimization feature disappears in the midfield and, on the ideal low-boom signature, leaves a plateau-shaped pressure wave.

The saw-tooth perturbations in the inviscid-theory signature, as compared with the inviscid boom-constrained theory signature, are due to the imperfect matching of the ideal and the model effective-area curves and to unavoidable, small, construction inaccuracies. These effects, plus those due to viscosity, appear in the viscous-corrected signatures; thus, none of the theoretical signatures are perfectly flat from nose shock to expansion point.

The agreement between theoretical and experimental signatures improves as the comparison signature changes from the inviscid, boom constrained to the inviscid and finally to the viscous corrected. Mach number effects are definitely present. At a Mach number of 1.5, the agreement between measured and predicted signatures is good from nose shock to tail shock; while at a Mach number of 2.7, the agreement is very good only from the nose shock to the compression peak just before the final expansion. The poor agreement on this aft section of the pressure signatures at M = 2.7 has been noted before at various Mach number and lift conditions such as those described in references 8, 15, and 16. Some of the wing and wing-body models in these references had

10

leading-edge sweep angles which changed, along the semispan, from subsonic to supersonic in character - as did the leading edges on the Mach 2.7 low-boom arrow-wing models. This type of leading edge might be producing the Δp increment between the measured and viscous-corrected signature levels which is seen on the preexpansion peaks in figures 14(a) and 14(b). It could also account for the changing character of this preexpansion peak that is seen in figure 13(b).

Thus, boundary-layer displacement-thickness correction accounts for most of the measured and inviscid theory signature differences at $M = 1.5$ and the major part of these differences at $M = 2.7$. However, possible inaccuracies in the prediction of the effective lift distribution, as well as the possibility that the limits of linearized theory are being approached, could be contributing to the poor agreement at the higher Mach number.

Since wind-tunnel-model pressure signatures are measured in the near field, estimates of ground overpressures are found by extrapolating theoretical signatures (based on model geometry) or measured signatures from a cruise altitude to the ground. In figure 15, both of these extrapolations are shown and compared at the test Mach numbers of 2.7 and 1.5. The ideal, boom-constrained signatures were provided by the minimization program; the viscous-flow model and inviscid-flow model theory signatures were calculated with the method of reference 9, while the extrapolated wind-tunnel signatures were obtained by using the method of reference 17.

Good agreement between the ideal and the model extrapolated signatures in the inviscid theory calculations is seen at both Mach numbers since this was the basis of the model design. Comparisons of extrapolated wind-tunnel and viscous theory signatures do not show a similar good agreement at $M = 2.7$ but do at $M = 1.5$. Since only boundary-layer displacement-thickness corrections were applied, the previous comments concerning the viscous-flow corrections in the near-field signature comparisons also apply in these extrapolated signature comparisons. Thus, the good results at $M = 1.5$ lead to the conclusion that at the lower supersonic Mach numbers, an aircraft designed such that its volume, lift, boundary layer, etc. are constrained by a minimization-theory effective-area curve will generate a ground-level signature almost identical to that predicted by theory. The limited agreement between theory and experiment at $M = 2.7$ suggests that the minimization theory is probably valid but that further study is needed to establish this as a firm conclusion.

CONCLUDING REMARKS

A wind-tunnel study was conducted with two reference models and three low-boom models which were designed with the Seebass and George sonic-boom minimization theory. The conclusion that the method was valid and applicable to the design of supersonic cruise aircraft was shown to be justified at the test Mach number of 1.5. Encouraging results were obtained at a Mach number of 2.7, but further work is needed to assess the theory up to this higher Mach number.

Pressure signatures from the low-boom models were found to be relatively insensitive to small differences in Mach number and lift conditions from the design point. Boundary-layer effects were found to be significant on the slender low-boom models which had appreciable wing areas and extended lift-development lengths. Corrections for these viscous effects significantly improved the agreement between the measured and the predicted signatures in the near field and between the extrapolated wind tunnel and the viscous corrected theory signature in the far field (cruise altitude condition).

Langley Research Center
National Aeronautics and Space Administration
Hampton, VA 23665
September 17, 1979

REFERENCES

1. Seebass, R.; and George, A. R.: Sonic-Boom Minimization. J. Acoust. Soc. America, vol. 51, no. 2, pt. 3, Feb. 1972, pp. 686-694.

2. Carlson, Harry W.; Barger, Raymond L.; and Mack, Robert J.: Application of Sonic-Boom Minimization Concepts in Supersonic Transport Design. NASA TN D-7218, 1973.

3. Whitham, G. B.: The Flow Pattern of a Supersonic Projectile. Commun. Pure & Appl. Math., vol. V, no. 3, Aug. 1952, pp. 301-348.

4. Walkden, F.: The Shock Pattern of a Wing-Body Combination, Far From the Flight Path. Aeronaut. Q., vol. IX, pt. 2, May 1958, pp. 164-194.

5. Carlson, Harry W.: Correlation of Sonic-Boom Theory With Wind-Tunnel and Flight Measurements. NASA TR R-213, 1964.

6. Jones, L. B.: Lower Bounds For Sonic Bangs. J. Roy. Aeronaut. Soc., vol. 65, no. 606, June 1961, pp. 433-436.

7. McLean, F. Edward: Some Nonasymptotic Effects On the Sonic Boom of Large Airplanes. NASA TN D-2877, 1965.

8. Carlson, Harry W.; McLean, F. Edward; and Shrout, Barrett L.: A Wind-Tunnel Study of Sonic-Boom Characteristics for Basic and Modified Models of a Supersonic Transport Configuration. NASA TM X-1236, 1966.

9. Hayes, Wallace D.; Haefeli, Rudolph C.; and Kulsrud, H. E.: Sonic Boom Propagation in a Stratified Atmosphere, With Computer Program. NASA CR-1299, 1969.

10. Darden, Christine M.: Minimization of Sonic-Boom Parameters in Real and Isothermal Atmospheres. NASA TN D-7842, 1975.

11. Darden, Christine M.: Sonic-Boom Minimization With Nose-Bluntness Relaxation. NASA TP-1348, 1979.

12. Monaghan, R. J.: An Approximate Solution of the Compressible Laminar Boundary Layer on a Flat Plate. R. & M. No. 2760, British A.R.C., 1953.

13. Harris, Roy V., Jr.: A Numerical Technique for Analysis of Wave Drag at Lifting Conditions. NASA TN D-3586, 1966.

14. Carlson, Harry W.; and Miller, David S.: Numerical Methods for the Design and Analysis of Wings at Supersonic Speeds. NASA TN D-7713, 1974.

15. Shrout, Barrett L.; Mack, Robert J.; and Dollyhigh, Samuel M.: A Wind-Tunnel Investigation of Sonic-Boom Pressure Distributions on Bodies of Revolution at Mach 2.96, 3.83, and 4.63. NASA TN D-6195, 1971.

16. Miller, David S.; Morris, Odell A.; and Carlson, Harry W.: Wind-Tunnel Investigation of Sonic-Boom Characteristics of Two Simple Wing Models at Mach Numbers From 2.3 to 4.63. NASA TN D-6201, 1971.

17. Thomas, Charles L.: Extrapolation of Sonic Boom Pressure Signatures by the Waveform Parameter Method. NASA TN D-6832, 1972.

14

TABLE I.- NUMERICAL DESCRIPTION OF AIRCRAFT USED FOR DESIGNING

TEST MODELS WAVE-DRAG PROGRAM FORMAT (REF. 12)

[Dimensions in m and m^2]

(a) Reference delta

1 -1 -1   -1 5 11 2 19 30 19 30

										Label
773.32										REFA
0.	10.	20.	30.	40.	50.	60.	70.	80.	90.	XAF10
100.										XAF11
28.194	1.981	0.000	34.168							WAFORG1
37.490	4.572	0.000	24.689							WAFORG2
43.891	9.754	0.000	17.678							WAFORG3
50.444	15.240	0.000	11.125							WAFORG4
58.217	21.641	0.000	3.353							WAFORG5
0.	.53	.94	1.24	1.43	1.5	1.43	1.24	.94	.53	WAFORD10
0.										WAFORD11
0.	.53	.94	1.24	1.43	1.5	1.43	1.24	.94	.53	WAFORD20
0.										WAFORD21
0.	.53	.94	1.24	1.43	1.5	1.43	1.24	.94	.53	WAFORD30
0.										WAFORD31
0.	.53	.94	1.24	1.43	1.5	1.43	1.24	.94	.53	WAFORD40
0.										WAFORD41
0.	.53	.94	1.24	1.43	1.5	1.43	1.24	.94	.53	WAFORD50
0.										WAFORD51
0.000	1.524	3.048	4.572	6.096	7.620	9.144	10.668	12.192	13.716	XFUS10
15.240	16.764	18.288	19.812	21.336	22.860	24.384	25.908	27.432	28.956	XFUS11
30.480	32.004	33.528	35.052	36.576	38.100	39.624	41.148	42.672	44.196	XFUS12
0.000	.465	1.068	1.858	2.769	3.716	4.664	5.621	6.578	7.525	FUSA10
8.408	9.244	9.941	10.554	11.037	11.427	11.752	11.910	11.984	11.984	FUSA11
11.966	11.929	11.892	11.845	11.752	11.724	11.706	11.687	11.687	11.687	FUSA12
44.196	45.720	47.244	48.768	50.292	51.816	53.340	54.864	56.388	57.912	XFUS20
59.436	60.960	62.484	64.008	65.532	67.056	68.580	70.104	71.628	73.152	XFUS21
74.676	76.200	77.724	79.248	80.772	82.296	83.820	85.344	86.868	88.392	XFUS22
11.687	11.641	11.594	11.520	11.390	11.241	11.037	10.777	10.498	10.191	FUSA20
9.811	9.458	9.095	8.659	8.659	8.659	8.659	8.659	8.659	8.659	FUSA21
8.659	8.659	8.659	8.659	8.659	8.659	8.659	8.659	8.659	8.659	FUSA22

TABLE I.- Continued

(b) Reference arrow

```
 1 -1 -1              -1  5 12  2 19 30 19 18

 982.45                                                              REFA
0.       5.      10.     20.     30.     40.     50.     60.     70.     80.      XAF10
90.     100.                                                         XAF12
 24.994  1.829  0.000 48.768                                        WAFORG1
 35.052  4.877  0.000 38.710                                        WAFORG2
 52.121  9.754  0.000 23.043                                        WAFORG3
 69.037 14.630  0.000  9.754                                        WAFORG4
 78.334 20.117  0.000  4.328                                        WAFORG5
0.       .575    .78    1.03    1.17    1.26    1.3     1.24    1.08     .82      WAFORD10
 .45     0.                                                          WAFORD12
0.       .575    .78    1.03    1.17    1.26    1.3     1.24    1.08     .82      WAFORD20
 .45     0.                                                          WAFORD22
0.       .575    .78    1.03    1.17    1.26    1.3     1.24    1.08     .82      WAFORD30
 .45     0.                                                          WAFORD32
0.       .575    .78    1.03    1.17    1.26    1.3     1.24    1.08     .82      WAFORD40
 .45     0.                                                          WAFORD42
0.       .575    .78    1.03    1.17    1.26    1.3     1.24    1.08     .82      WAFORD50
 .45     0.                                                          WAFORD52
  0.000   3.048   6.096   9.144  12.192  15.240  18.288  21.336  24.384  27.432  XFUS10
 30.480  33.528  36.576  39.624  42.672  45.720  48.768  51.816  54.864  57.912  XFUS20
 60.960  64.008  67.056  70.104  73.152  76.200  79.248  82.296  85.344  88.392  XFUS30
  0.000   1.115   2.880   4.738   6.503   8.268   9.848  11.241  11.613  11.474  FUSA10
 10.870  10.312   9.848   9.755   9.848   9.894   9.941   9.941   9.848   9.708  FUSA20
  9.476   9.012   8.547   7.711   6.689   5.481   5.481   5.481   5.481   5.481  FUSA30
 88.392  91.440  94.488  97.536100.584103.632106.680109.728112.776115.824       XFUS40
118.872121.920124.968128.016131.064134.112137.160140.208                        XFUS50
  5.481   5.481   5.481   5.481   5.481   5.481   5.481   5.481   5.481   5.481  FUSA40
  5.481   5.481   5.481   5.481   5.481   5.481   5.481   5.481                  FUSA50
```

16

TABLE I.- Continued

(c) Mach 2.7 low-boom arrow

```
 1 -1 -1              -1   5  11   3  19  20  19  20  19  25
```

1482.73										REFA
0.	10.	20.	30.	40.	50.	60.	70.	80.	90.	XAF 10
100.										XAF 11
17.526	2.286	.295	65.627							WAFORG 1
54.864	9.754	1.262	31.090							WAFORG 2
64.008	12.192	1.578	22.860							WAFORG 3
71.018	14.630	1.893	16.764							WAFORG 4
86.868	24.384	3.156	4.572							WAFORG 5
0.	.378	.672	.882	1.008	1.050	1.008	.882	.672	.378	WAFORD10
0.										WAFORD11
0.	.353	.635	.852	.975	1.023	1.005	.873	.675	.394	WAFORD20
0.										WAFORD21
0.	.400	.698	.908	1.044	1.093	1.080	.958	.737	.453	WAFORD30
0.										WAFORD31
0.	.464	.782	1.032	1.186	1.266	1.225	1.075	.820	.545	WAFORD40
0.										WAFORD41
0.	.658	1.100	1.400	1.625	1.716	1.725	1.583	1.350	.992	WAFORD50
0.										WAFORD51
0.000	1.524	3.048	4.572	6.096	7.620	9.144	10.668	12.192	13.716	XFUS 10
15.240	16.764	18.288	19.812	21.336	22.860	24.384	25.908	27.432	28.956	XFUS 11
0.000	.074	.307	.901	2.573	4.069	5.583	7.116	8.556	9.857	FUSA 10
11.055	12.161	13.202	14.121	14.920	15.728	16.332	16.815	17.168	17.419	FUSA 11
28.956	30.480	32.004	33.528	35.052	36.576	38.100	39.624	41.148	42.672	XFUS 20
44.196	45.720	47.244	48.768	50.292	51.816	53.340	54.864	56.388	57.912	XFUS 21
17.419	17.549	17.577	17.512	17.391	17.326	17.196	16.927	16.750	16.527	FUSA 20
16.332	16.091	15.831	15.598	15.366	15.152	14.967	14.632	14.298	13.917	FUSA 21
57.912	59.436	60.960	62.484	64.008	65.532	67.056	68.580	70.104	71.628	XFUS 30
73.152	74.676	76.200	77.724	79.248	80.772	82.296	83.820	85.344	86.868	XFUS 31
88.392	89.916	91.440	92.964	94.488						XFUS 32
13.917	13.499	13.118	12.542	11.957	11.492	10.898	10.349	9.838	9.383	FUSA 30
8.928	8.463	7.980	7.534	7.079	6.652	6.206	5.797	5.444	5.091	FUSA 31
4.785	4.589	4.227	4.116	4.041						FUSA 32

TABLE I.- Continued

(d) Mach 2.7 low-boom blunt-apex arrow[a]

```
  1 -1 -1              -1   9  11   3  19  20  19  20  19  27

1541.91                                                                  REFA
0.      10.     20.     30.     40.     50.     60.     70.     80.     90.      XAF 10
100.0                                                                    XAF 11
     4.478   1.829    .297  82.086                                       WAFORG1
     6.096   2.134    .346  80.467                                       WAFORG2
    13.716   3.200    .519  72.847                                       WAFORG3
    22.860   4.267    .693  63.703                                       WAFORG4
    51.511   8.534   1.385  36.271                                       WAFORG5
    60.960  10.668   1.731  27.432                                       WAFORG6
    68.275  12.802   2.078  20.726                                       WAFORG7
    74.066  14.935   2.424  15.545                                       WAFORG8
    86.868  21.336   3.463   4.572                                       WAFORG9
0.0     .36     .64     .84     .96    1.0     .96     .84     .64     .36      WAFORD10
0.0                                                                      WAFORD11
0.      .365    .634    .842    .958    .991    .956    .842    .644    .362     WAFORD20
0.0                                                                      WAFORD21
0.      .364    .634    .839    .957    .993    .957    .842    .643    .359     WAFORD30
0.0                                                                      WAFORD31
0.      .366    .654    .852    .966   1.001    .966    .844    .643    .367     WAFORD40
0.0                                                                      WAFORD41
0.      .381    .675    .895   1.014   1.046   1.012    .888    .673    .383     WAFORD50
0.0                                                                      WAFORD51
0.      .389    .703    .920   1.058   1.104   1.070    .927    .699    .526     WAFORD60
0.0                                                                      WAFORD61
0.      .434    .752    .987   1.155   1.203   1.149   1.000    .758    .439     WAFORD70
0.0                                                                      WAFORD71
0.      .459    .833   1.111   1.245   1.297   1.248   1.089    .851    .532     WAFORD80
0.                                                                       WAFORD81
0.     1.292   1.792   2.067   2.242   2.259   2.158   2.033   1.667   1.100     WAFORD90
0.0                                                                      WAFORD91
   0.000   1.524   3.048   4.572   6.096   7.620   9.144  10.668  12.192  13.716   XFUS 10
  15.240  16.764  18.288  19.812  21.336  22.860  24.384  25.908  27.432  28.956   XFUS 11
   0.000    .160    .463    .846   1.682   2.863   4.078   5.316   6.349   7.206   FUSA 10
   7.884   8.547   9.154   9.684  10.135  10.559  10.878  11.057  11.255  11.401   FUSA 11
  28.956  30.480  32.004  33.528  35.052  36.576  38.100  39.624  41.148  42.672   XFUS 20
  44.196  45.720  47.244  48.768  50.292  51.816  53.340  54.864  56.388  57.912   XFUS 21
  11.401  11.584  11.584  11.603  11.603  11.603  11.621  11.621  11.621  11.621   FUSA 20
  11.621  11.621  11.621  11.603  11.603  11.603  11.603  11.603  11.584  11.639   FUSA 21
  57.912  59.436  60.960  62.484  64.008  65.532  67.056  68.580  70.104  71.628   XFUS 30
  73.152  74.676  76.200  77.724  79.248  80.772  82.296  83.820  85.344  86.868   XFUS 31
  88.392  89.916  91.440  92.964  94.488  96.012  97.536                           XFUS 32
  11.639  11.584  11.565  11.419  11.274  11.003  10.860  10.542  10.194   9.903   FUSA 30
   9.400   8.829   8.245   7.726   7.137   6.613   6.176   5.793   5.422   5.124   FUSA 31
   4.799   4.600   4.439   4.281   4.159   4.126   4.104                           FUSA 32.
```

[a]$0 \leqq y \leqq 3.2004$; $x_{le} = 13.716(y/3.2004)^2$.

18

TABLE I.- Concluded

(e) Mach 1.5 low-boom arrow

```
  1 -1 -1   0   0   0  -1  11  11   3  19  21  19  21  19  24

1405.34                                                              REFA
0.      10.     20.     30.     40.     50.     60.     70.     80.     90.     XAF 10
100.                                                                 XAF 11
  19.159  1.676   .380  71.062                                       WAFORG1
  24.384  2.134   .484  65.532                                       WAFORG2
  33.528  4.267   .967  56.388                                       WAFORG3
  43.282  6.401  1.451  46.634                                       WAFORG4
  53.340  8.534  1.935  36.576                                       WAFORG5
  63.398 10.668  2.419  26.771                                       WAFORG6
  71.933 12.802  2.903  18.492                                       WAFORG7
  77.114 14.935  3.386  13.564                                       WAFORG8
  80.467 17.069  3.870  10.464                                       WAFORG9
  83.515 19.202  4.354   7.672                                       WAFORG10
  86.868 21.336  4.838   4.572                                       WAFORG11
0.0     .36     .64     .84     .96    1.0     .96     .64     .64     .36     WAFORD 1
0.0                                                                  WAFORD 1
0.0     .371    .644    .860    .983   1.030   .995    .873    .666    .384    WAFORD 2
0.0                                                                  WAFORD 2
0.0     .403    .705    .934   1.072   1.120   1.081   .951    .722    .414    WAFORD 3
0.0                                                                  WAFORD 3
0.0     .432    .761   1.012   1.167   1.221   1.185   1.037   .783    .449    WAFORD4
0.0                                                                  WAFORD 4
0.0     .472    .818   1.082   1.256   1.321   1.283   1.128   .849    .448    WAFORD 5
0.0                                                                  WAFORD 5
0.0     .528    .889   1.174   1.365   1.440   1.395   1.213   .902    .537    WAFORD 6
0.0                                                                  WAFORD 6
0.0     .593   1.012   1.333   1.523   1.585   1.523   1.308   .985    .598    WAFORD 7
0.0                                                                  WAFORD 7
0.0     .674   1.098   1.410   1.607   1.674   1.612   1.385   1.056   .643    WAFORD 8
0.0                                                                  WAFORD 8
0.0     .746   1.194   1.504   1.700   1.784   1.722   1.489   1.169   .721    WAFORD 9
0.0                                                                  WAFORD 9
0.0     .830   1.272   1.604   1.848   1.942   1.843   1.614   1.267   .800    WAFORD10
0.0                                                                  WAFORD10
0.0     .883   1.425   1.842   2.050   2.058   1.958   1.750   1.367   .867    WAFORD11
0.0                                                                  WAFORD11
  0.000  1.524  3.048  4.572  6.096  7.620  9.144 10.668 12.192 13.716 XFUS10
 15.240 16.764 18.288 19.812 21.336 22.860 24.384 25.908 27.432 28.956 XFUS11
 30.480                                                              XFUS12
  0.000   .092   .353   .776  1.394  2.065  2.886  3.825  4.764  5.599 FUSA 10
  6.502  7.370  8.183  8.974  9.616 10.298 10.825 11.201 11.565 11.880 FUSA 11
 12.124                                                              FUSA 12
 30.480 32.004 33.528 35.052 36.576 38.100 39.624 41.148 42.672 44.196 XFUS20
 45.720 47.244 48.768 50.292 51.816 53.340 54.864 56.388 57.912 59.436 XFUS21
 60.960                                                              XFUS22
 12.124 12.351 12.503 12.656 12.733 12.752 12.771 12.618 12.503 12.369 FUSA 20
 12.236 11.918 11.639 11.328 11.057 10.789 10.525 10.454 10.194  9.988 FUSA 21
  9.836                                                              FUSA 22
 60.960 62.484 64.008 65.532 67.056 68.580 70.104 71.628 73.152 74.676 XFUS30
 76.200 77.724 79.248 80.772 82.296 83.820 85.344 86.868 88.392 89.916 XFUS31
 91.440 92.964 94.488 96.012                                        XFUS32
  9.836  9.717  9.583  9.466  9.334  9.185  9.185  9.185  9.153  9.185 FUSA 30
  9.153  9.136  9.136  9.104  9.136  9.104  8.813  8.167  7.355  6.002 FUSA 31
  4.140  4.140  4.140  4.140                                        FUSA 32
```

TABLE II.- ANGLE-OF-ATTACK AND PRISM-ANGLE SETTINGS

Model	Mach number							
	1.5		2.6		2.7		2.8	
	α	θ	α	θ	α	θ	α	θ
Reference delta	3°27'	2°5'	—	—	3°26'	2°51'	—	—
Reference arrow	4°14'	3°0'	—	—	2°46'	2°14'	—	—
M=2.7 Low-boom arrow	—	—	1°46'	1°12'	1°38'	1°6'	1°34'	1°6'
	—	—	2°13'	1°30'	2°2'	1°23'	1°57'	1°22'
	—	—	2°40'	1°48'	2°27'	1°40'	2°21'	1°38'
M=2.7 Low-boom blunt-apex arrow	—	—	—	—	1°48'	1°12'	—	—
	—	—	—	—	2°15'	1°30'	—	—
	—	—	—	—	2°42'	1°48'	—	—
M=1.5 Low-boom arrow	2°42'	1°32'	—	—	—	—	—	—
	3°23'	1°56'	—	—	—	—	—	—
	4°3'	2°19'	—	—	—	—	—	—

— Test not made

● Test made but data not used in report

▶ Angle which theoretically produces a full-scale lift of 272 155 kg (600 000 lb)
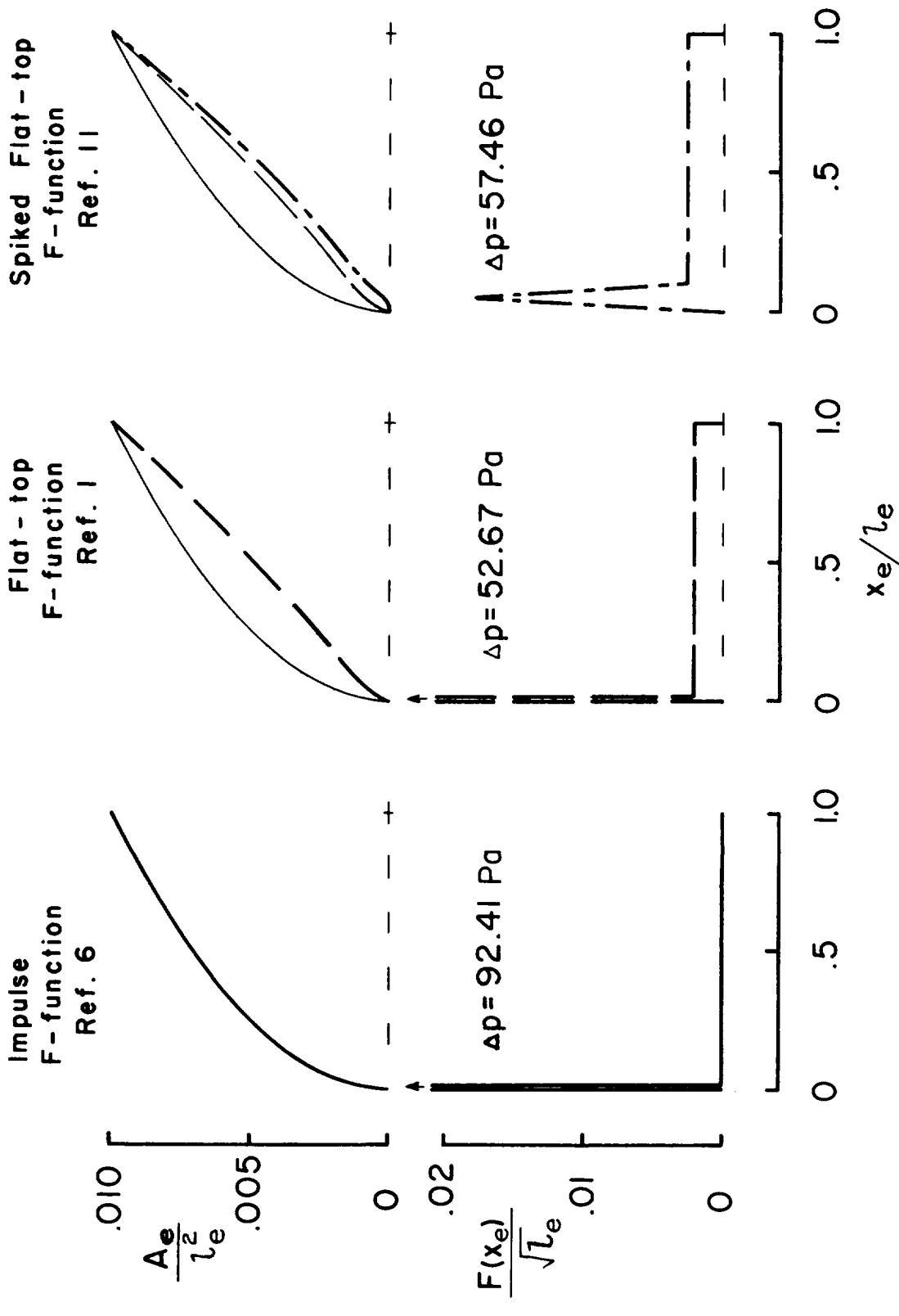
Figure 1.- Effective area and F-functions from minimization methods of references 1, 6, and 11. Δp is calculated for h = 18 288 m (60 000 ft).

M=1.5 Low-Boom
Arrow

M=2.7 Low-Boom
Blunt-Apex Arrow

M=2.7 Low-Boom
Arrow

Unconstrained
Arrow

Unconstrained
Delta
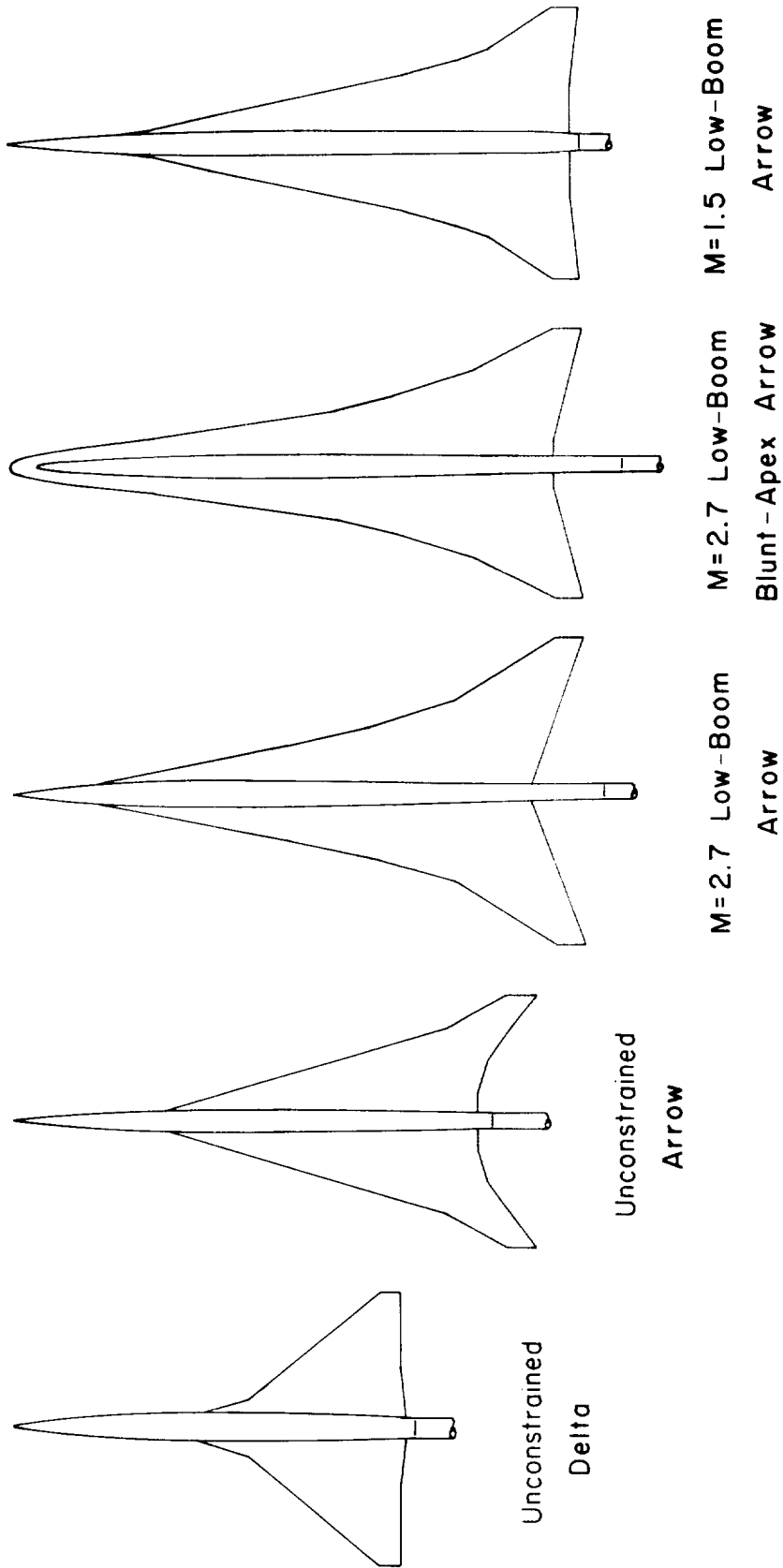
Figure 2.- Models used in sonic-boom minimization study.
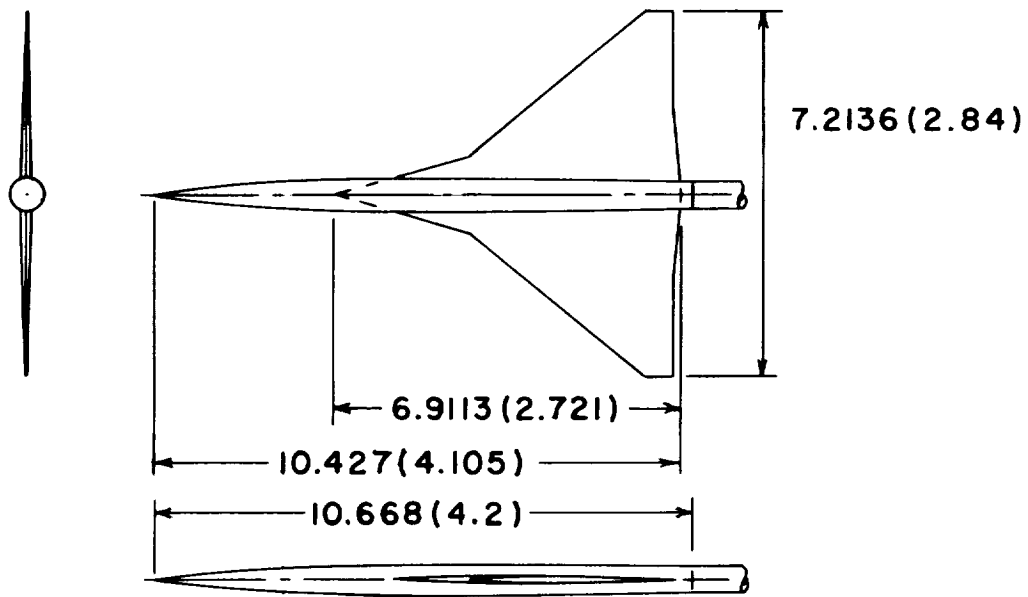
(a) Reference delta-wing model.
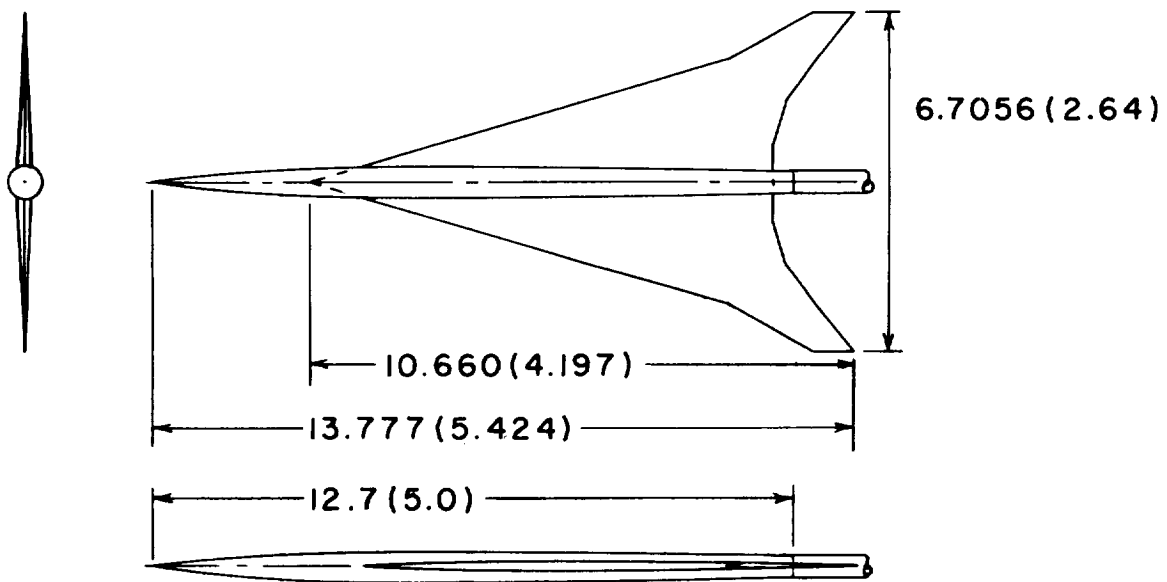
(b) Reference arrow-wing model.

Figure 3.- Unconstrained wind-tunnel models. Dimensions in cm (in.).
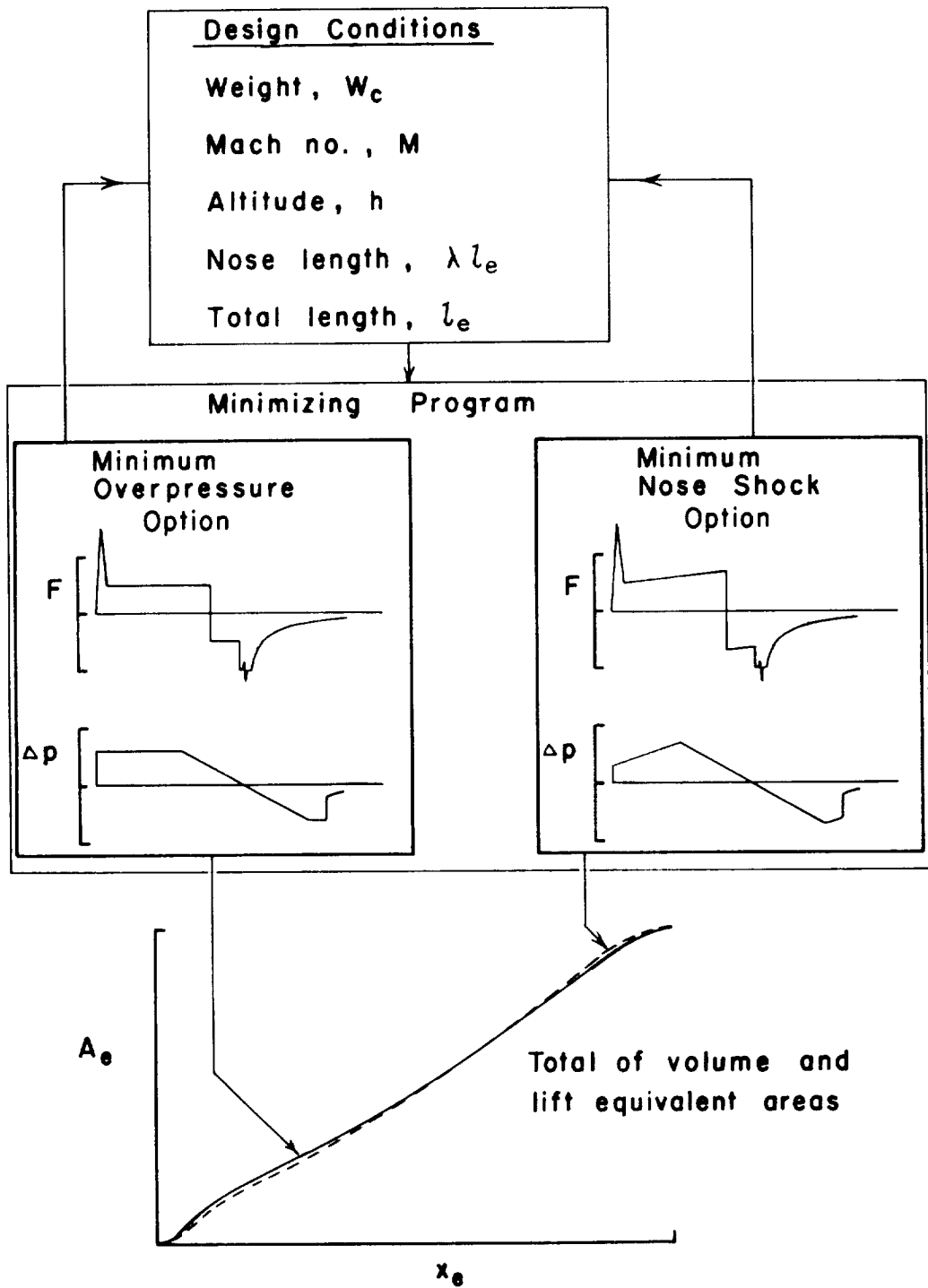
Figure 4.- Schematic outline of minimization process.
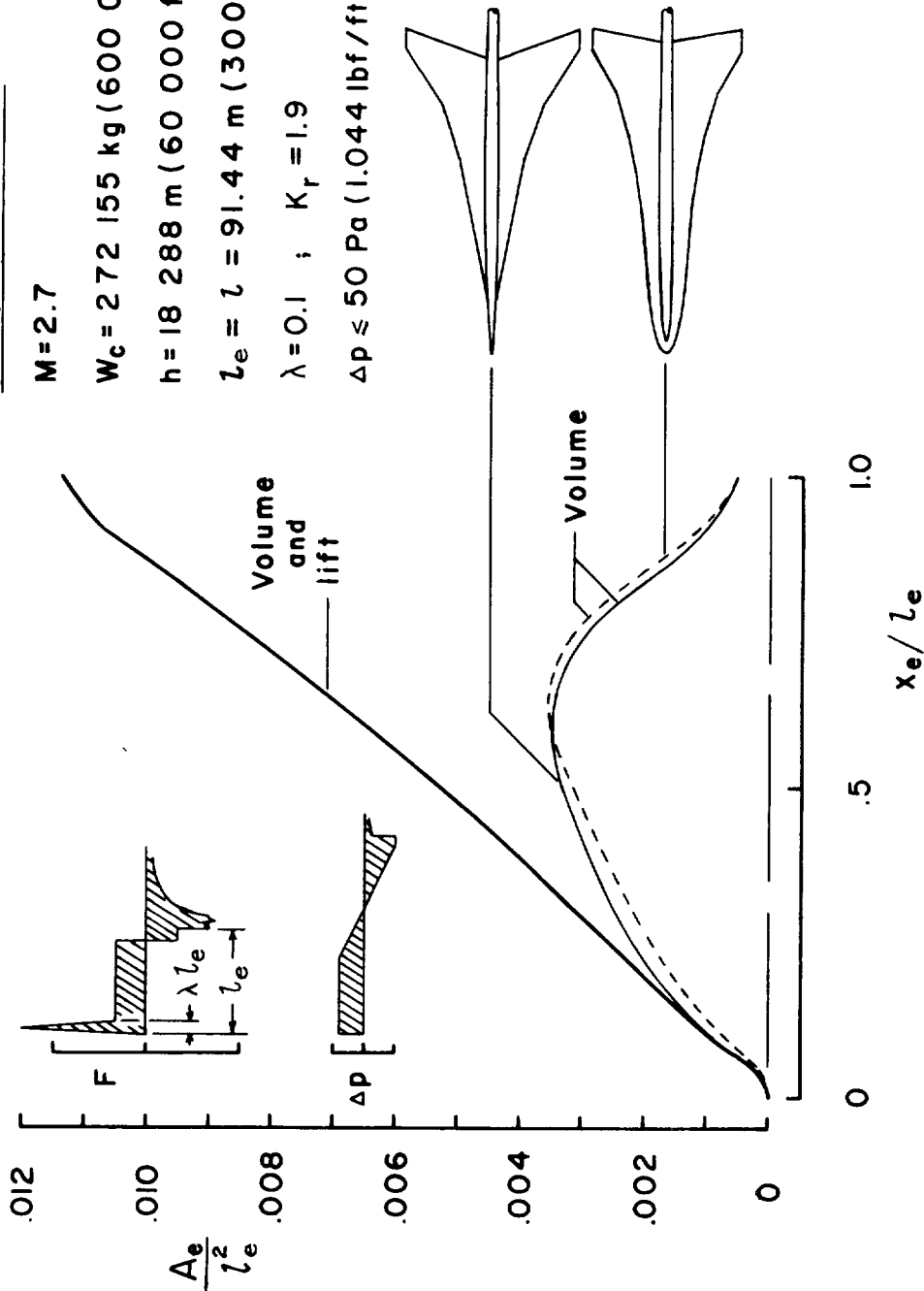
Figure 5.- Example of design procedure for two models which give specified minimum boom at M = 2.7.

Blunted, boom contoured nose section

Highly swept leading edge

Area-ruled fuselage

Varying thickness ratio wing

Wing dihedral

Long effective length

Extensive lifting surface
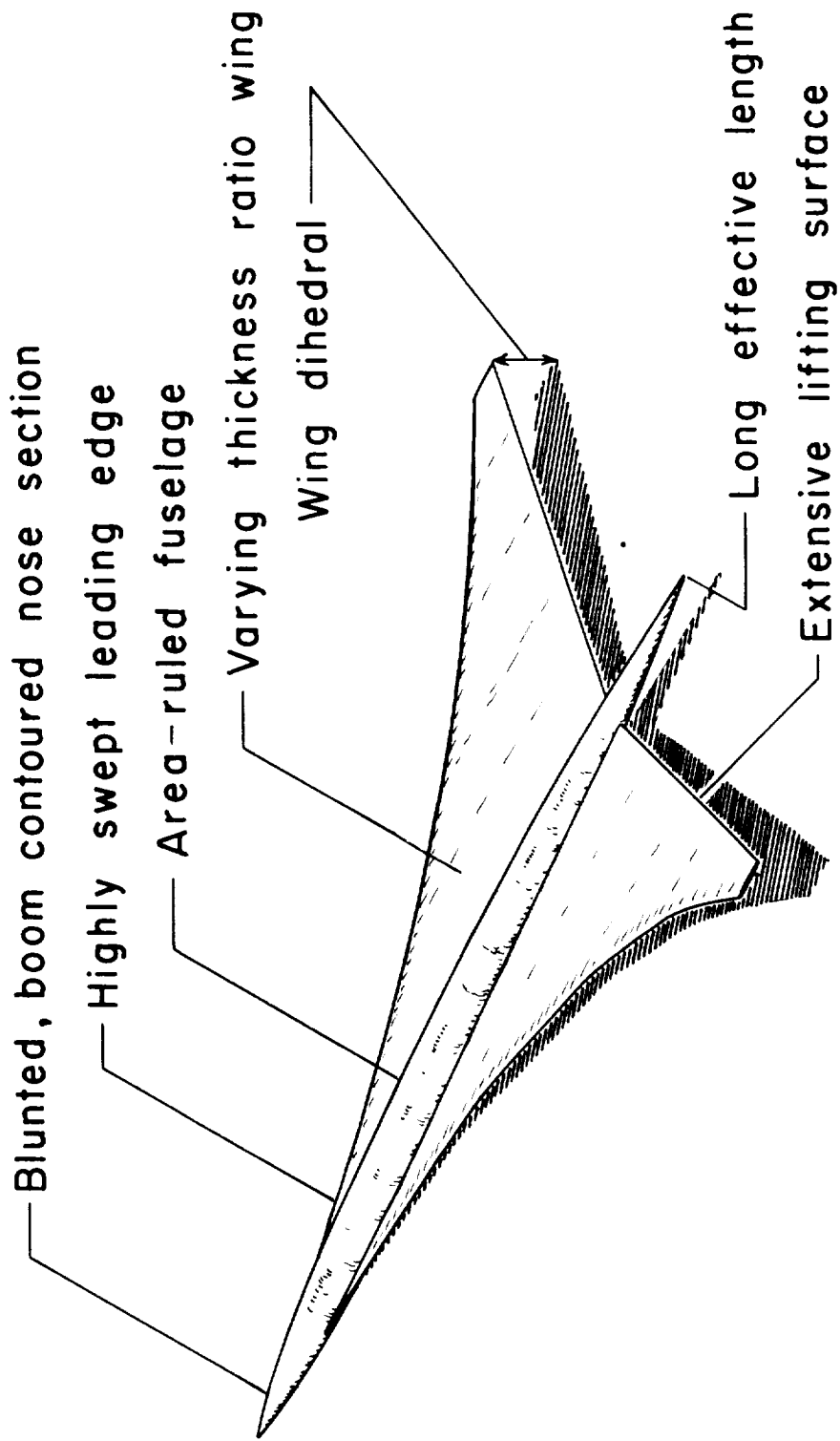
Figure 6.- Features of low-boom study models.
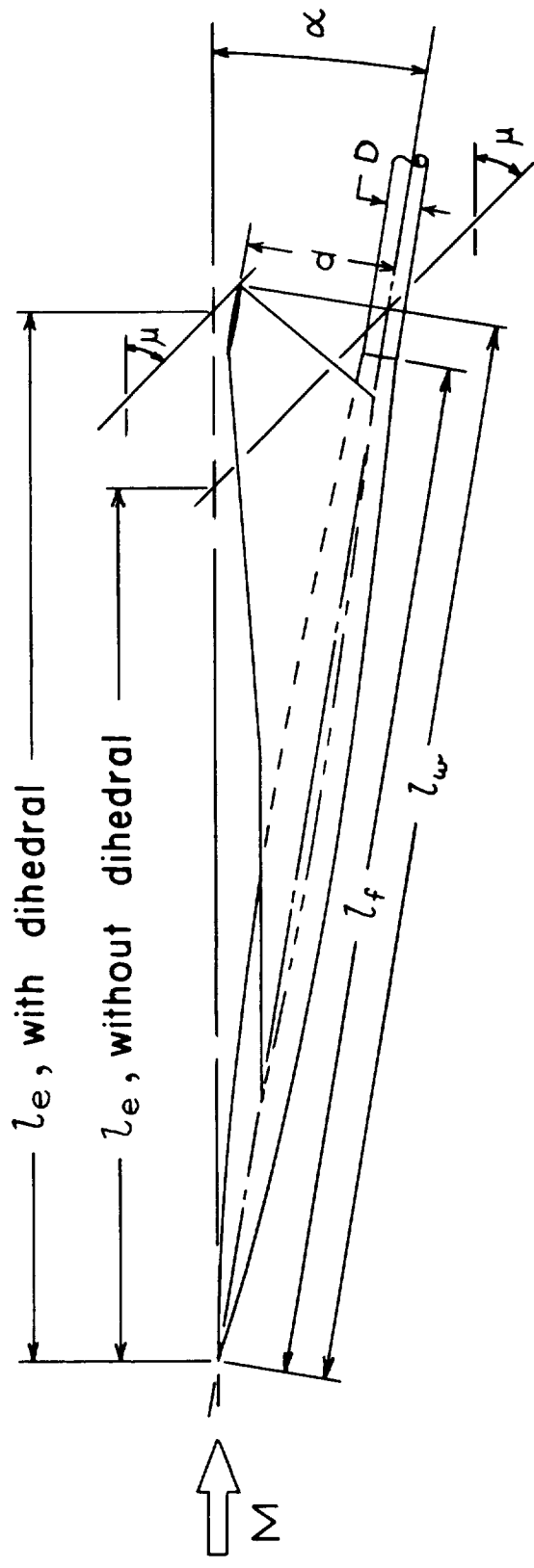
$$l_e = l_w \cos\alpha \left(1 - \beta \tan\alpha \right) + d \cos\alpha \left(\beta + \tan\alpha \right)$$

Figure 7.- Side view of model showing effect of dihedral on effective length.

27
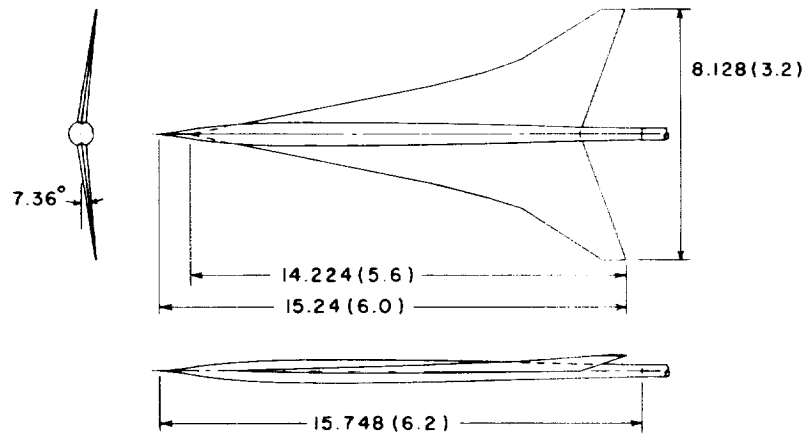
(a) Arrow-wing model designed for minimum boom at M = 2.7.
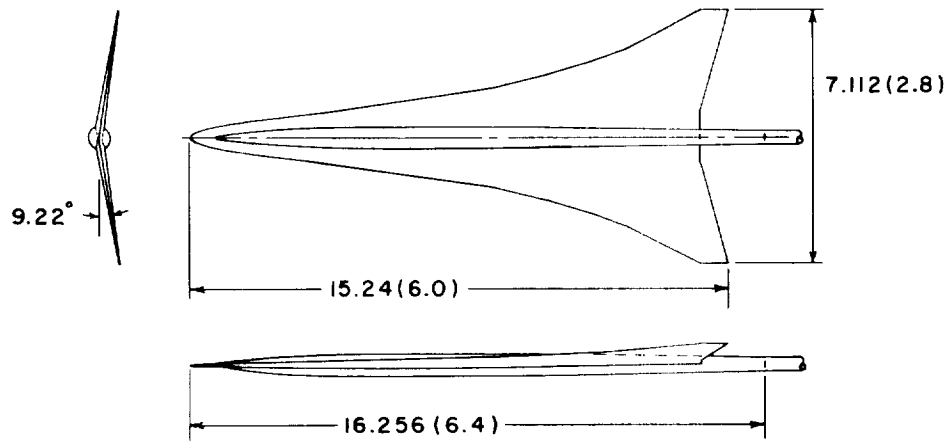
(b) Blunted arrow-wing model designed for minimum boom at M = 2.7.
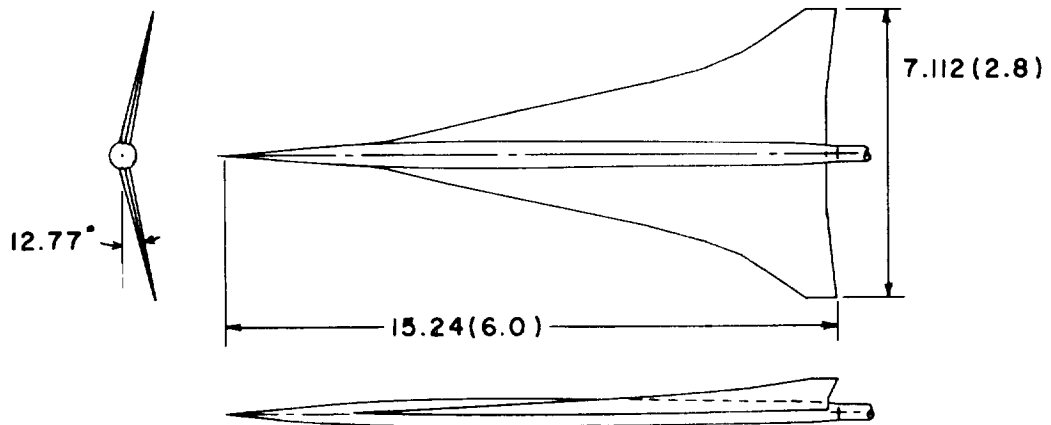
(c) Arrow-wing model designed for minimum boom at M = 1.5.

Figure 8.- Low-boom wind-tunnel models. Dimensions in cm (in.).

28

$\alpha = \theta + \Delta\alpha$
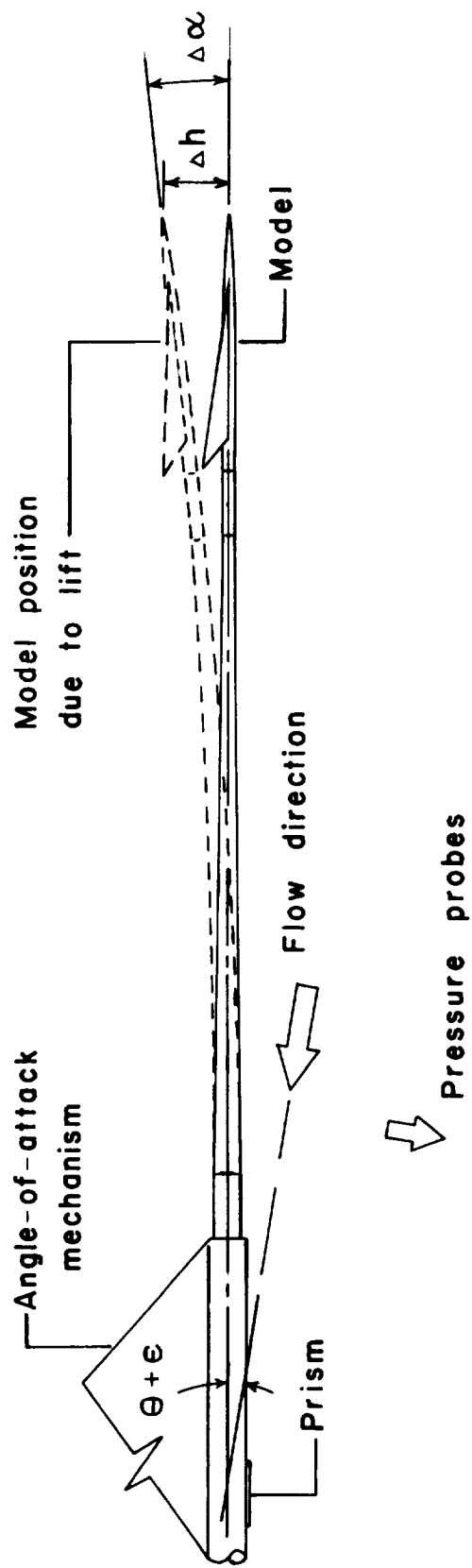
$\Delta\alpha = k \, C_{L_\alpha} \alpha \, q \, S$

$k = \Delta\alpha / \Delta L \quad$ from figure 9(b)

$\theta = \alpha \left(1.0 - k \, C_{L_\alpha} \, q \, S \right)$

(a) Schematic of model, sting, and sting support.

Figure 9.- Corrections due to sting flexure.

29

Model

Reference delta ————————

Reference arrow — — — — —

M=2.7   Low – boom   arrow   - - - - - - -

M=2.7   Low – boom   blunted   arrow   —·—·—·—··

M=1.5   Low – boom   arrow   — —· — —· —
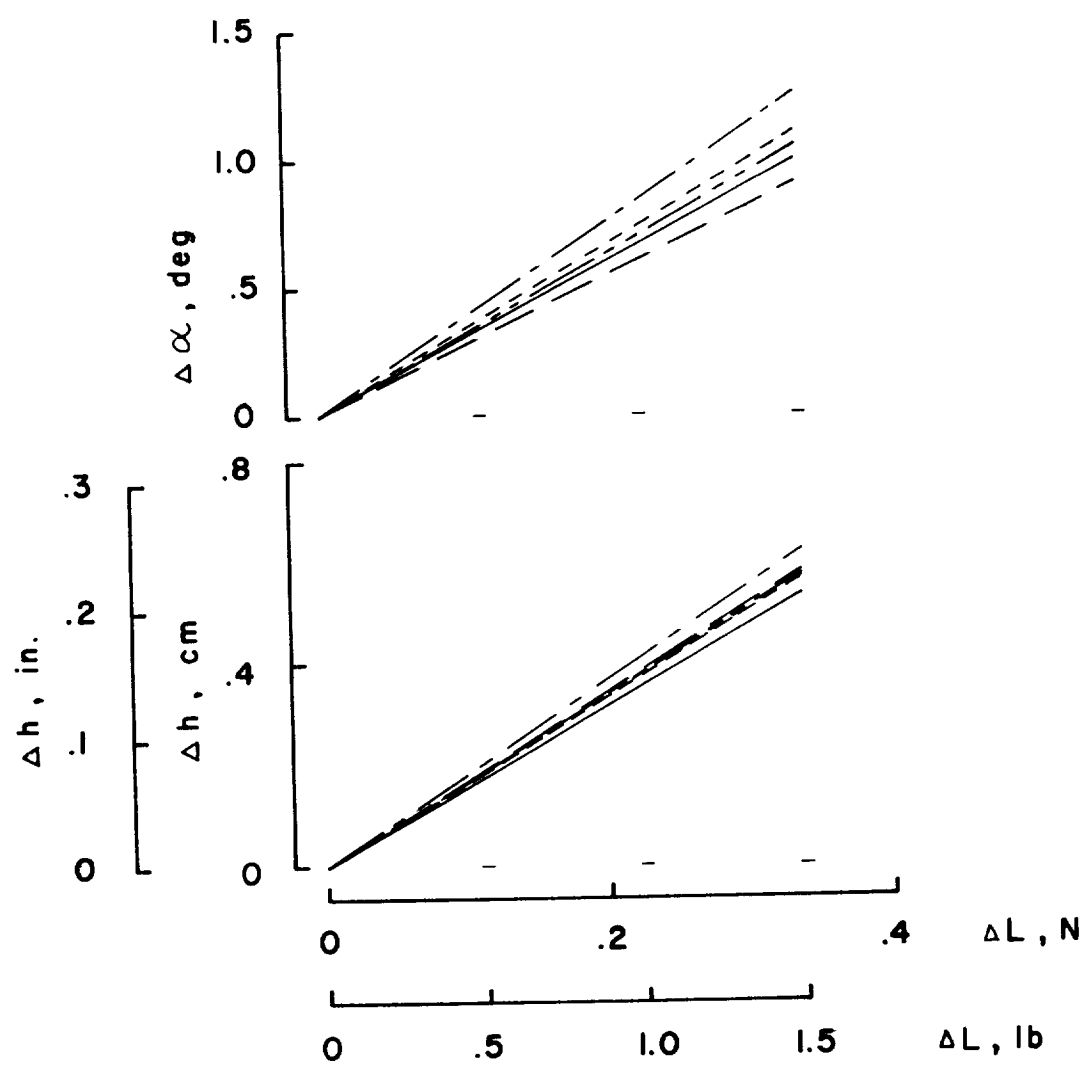
(b) Deflection curves.

Figure 9.- Concluded.
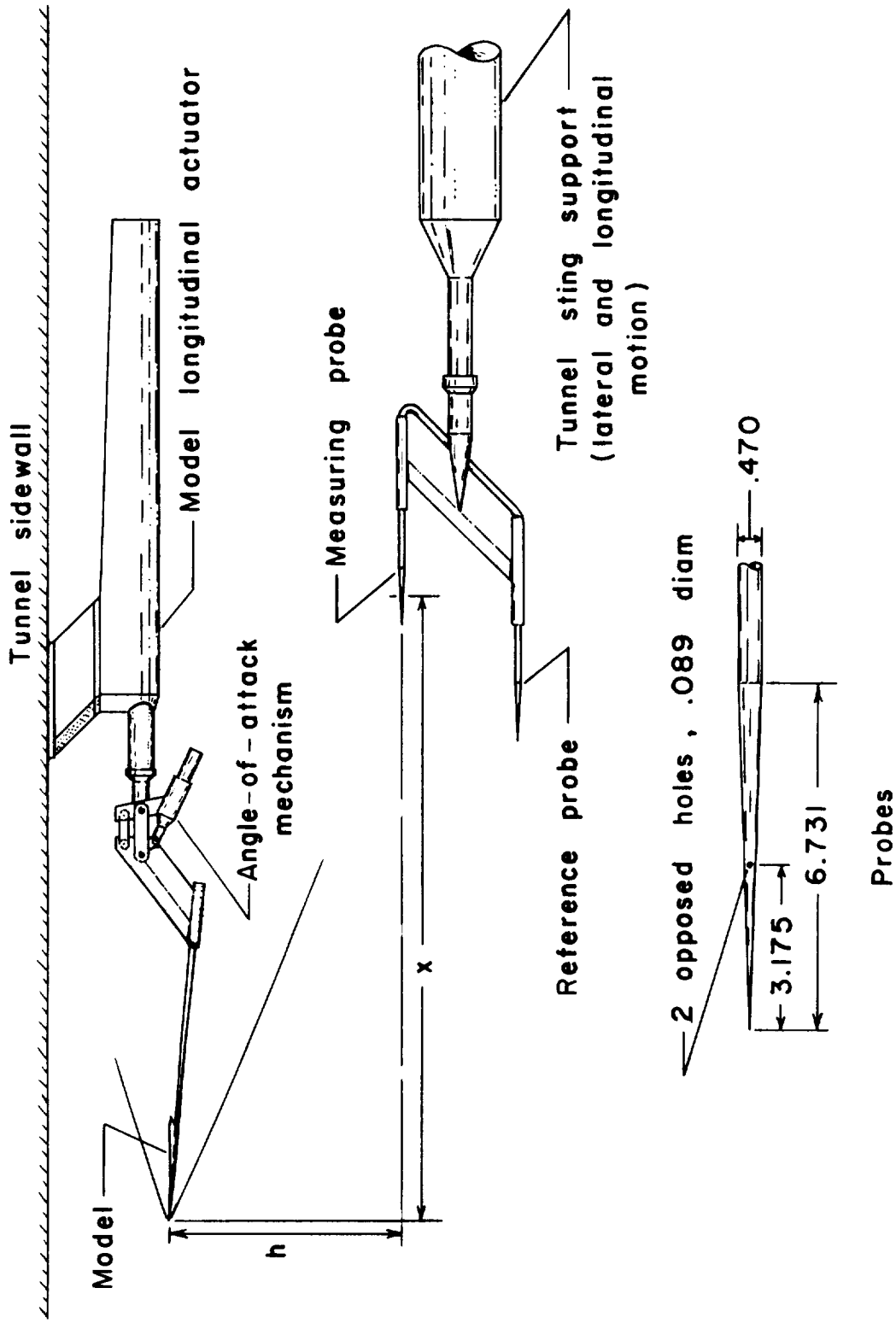
Figure 10.- Schematic of test apparatus. All dimensions are in centimeters.
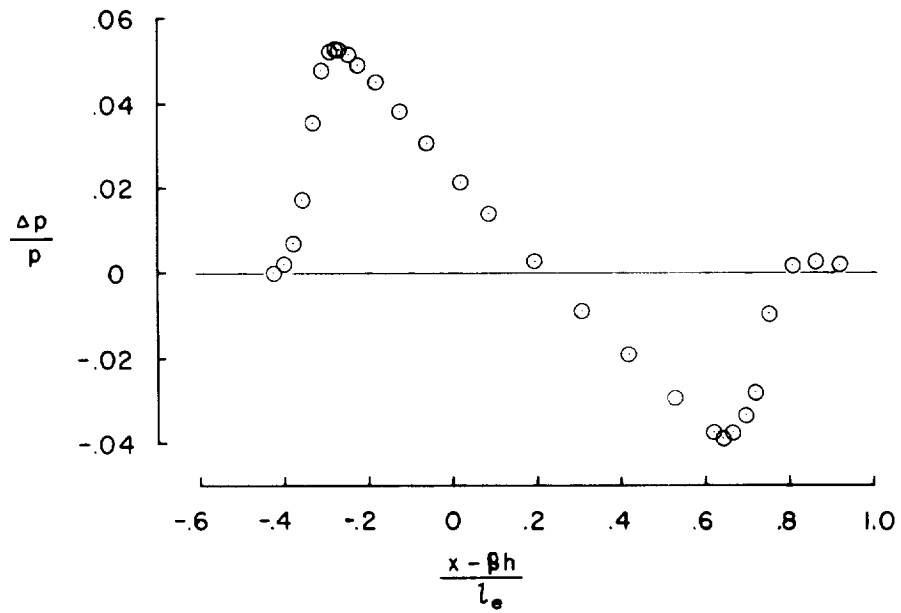
(a) Reference delta-wing model.
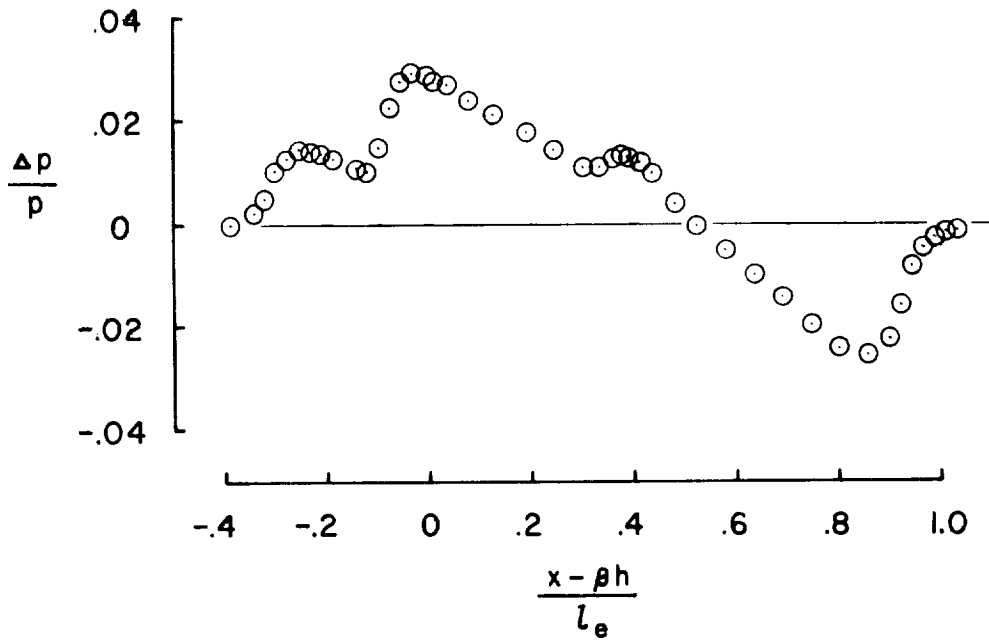
(b) Reference arrow-wing model.

Figure 11.- Measured pressure signatures at $M = 2.7$, $\alpha = \alpha_D$, and $h/l_e = 3$.
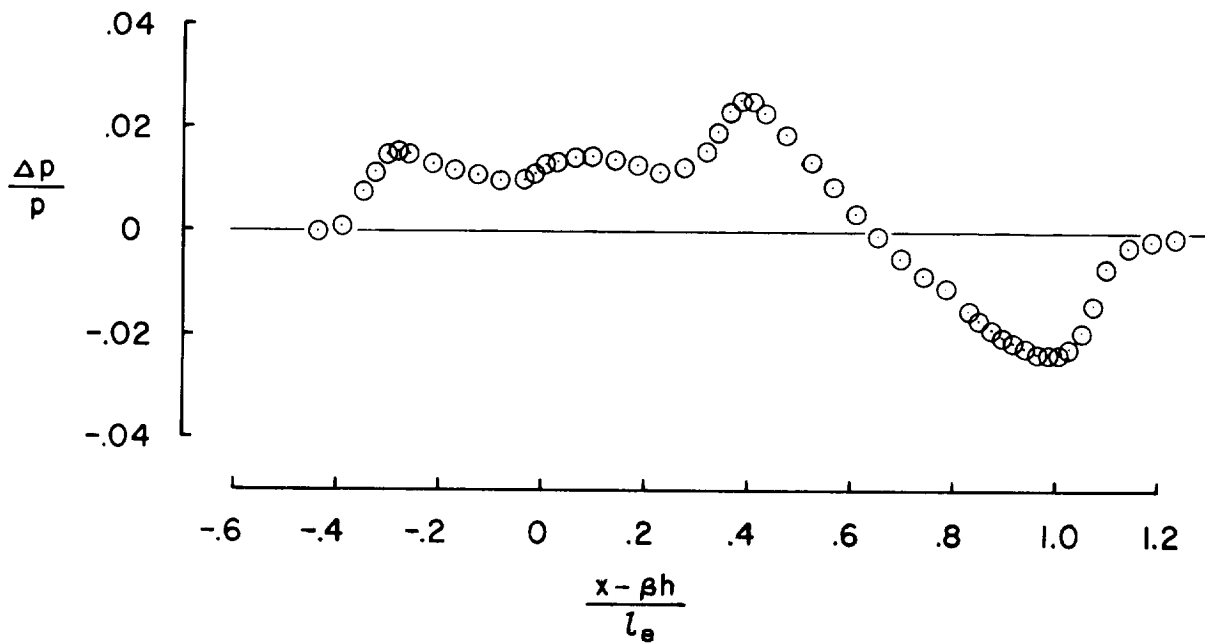
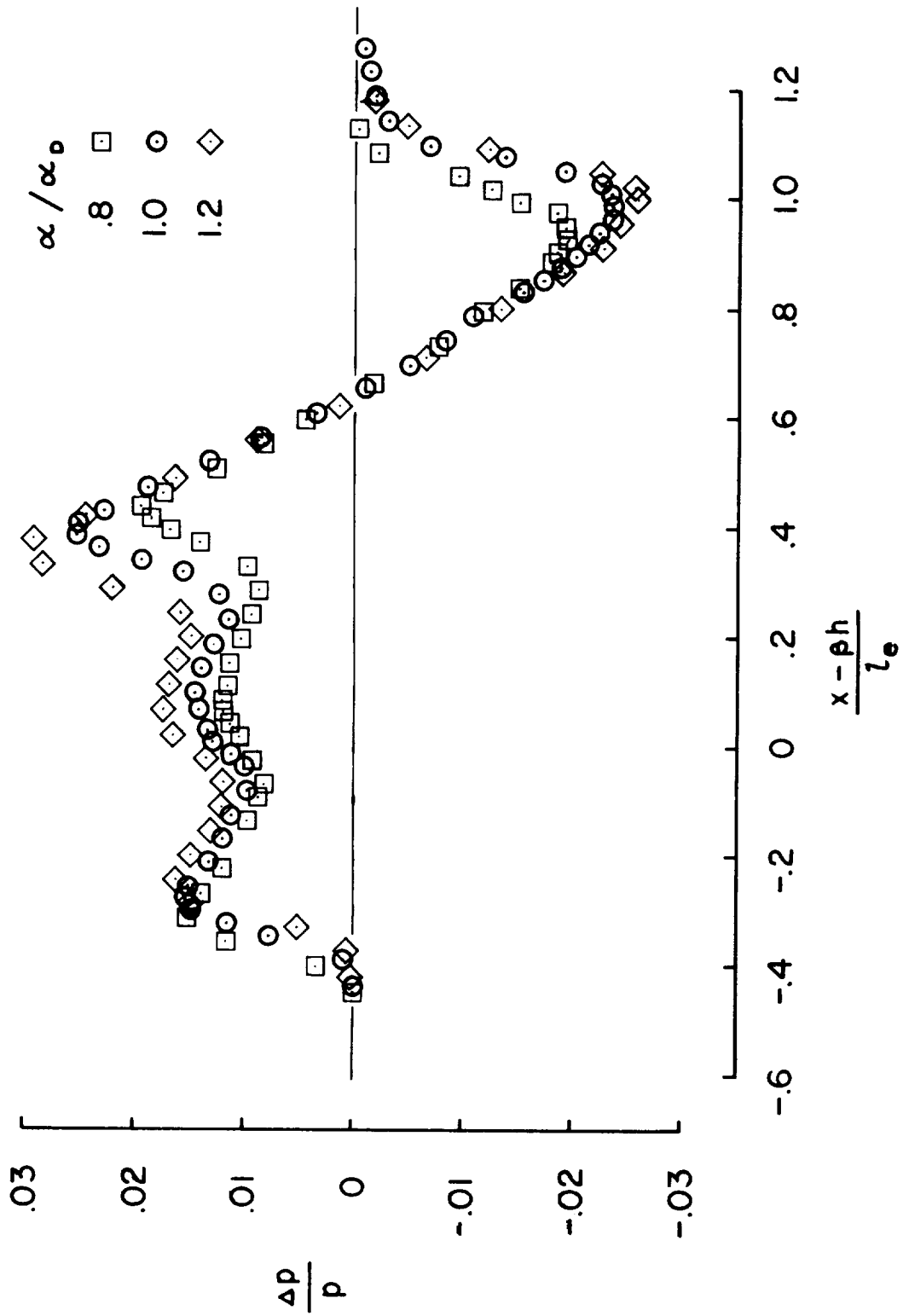(c) Mach 2.7 low-boom arrow-wing model.
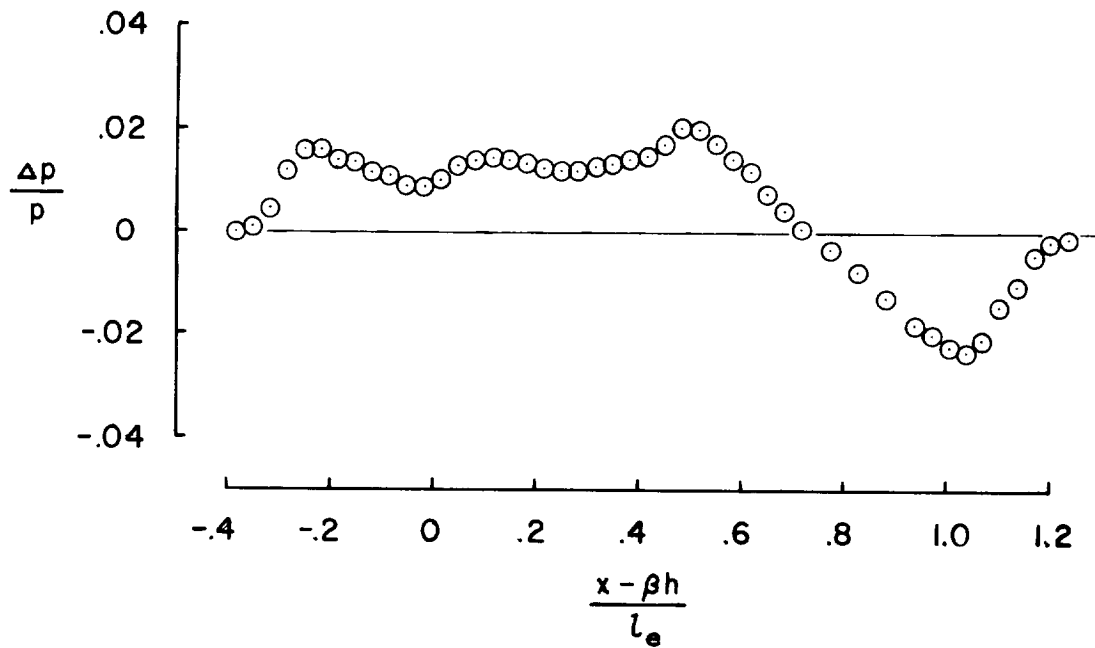
(d) Mach 2.7 low-boom blunt-apex arrow-wing model.

Figure 11.- Continued.
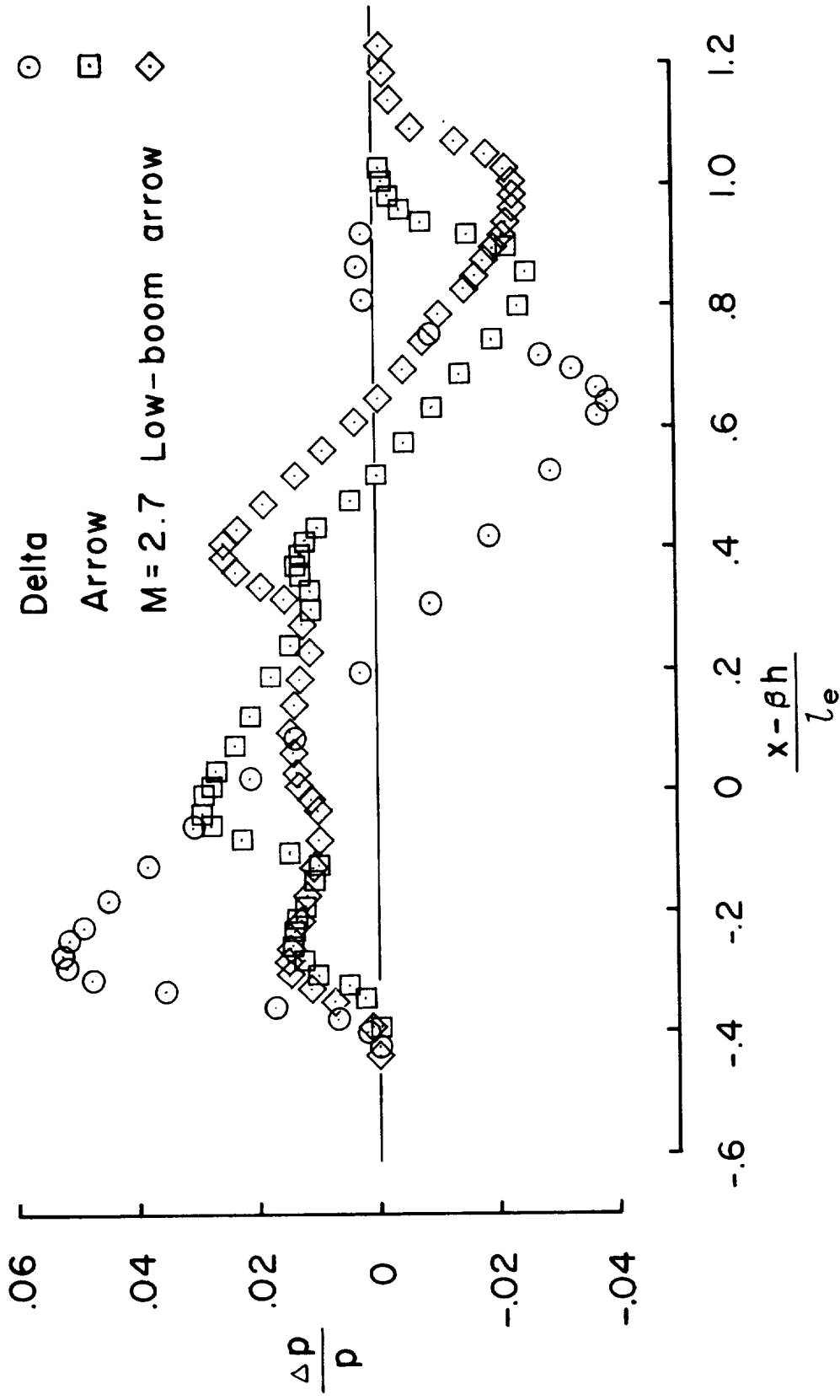
(e) Reference models and Mach 2.7 low-boom arrow-wing model.

Figure 11.- Continued.

34
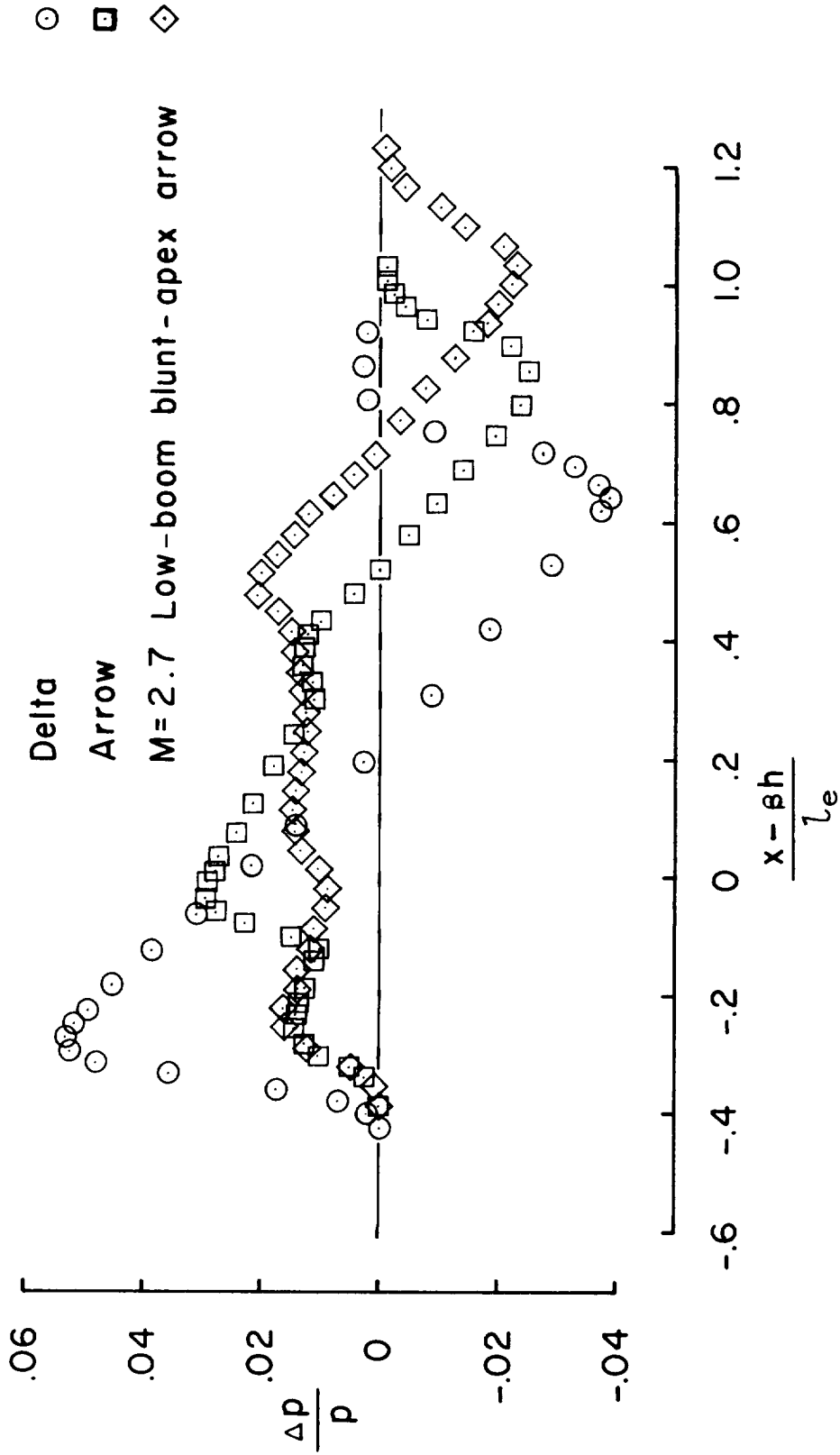
(f) Reference models and Mach 2.7 low-boom blunt-apex arrow-wing model.

Figure 11.- Concluded.

35
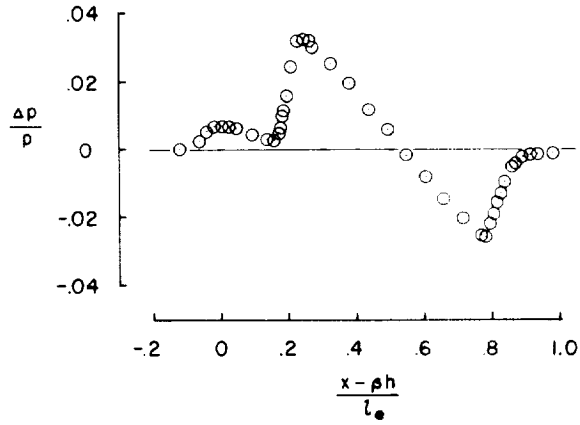
(a) Reference delta-wing model.
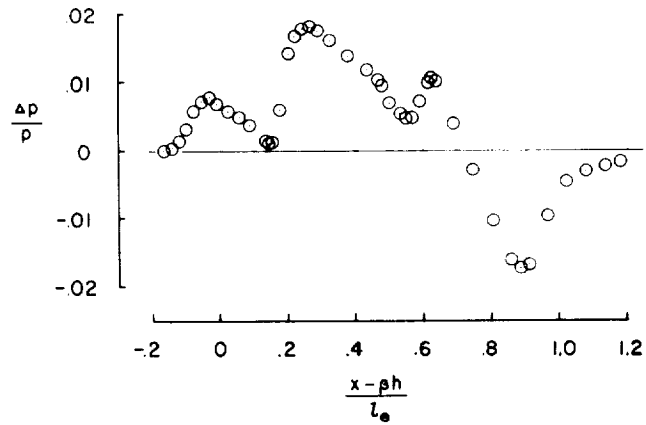
(b) Reference arrow-wing model.
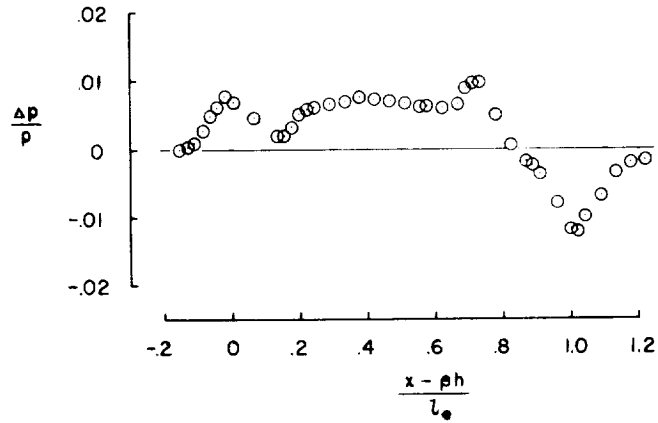
(c) Mach 1.5 low-boom arrow-wing model.

Figure 12.- Measured pressure signatures at $M = 1.5$, $\alpha = \alpha_D$, and $h/l_e = 3$.

36
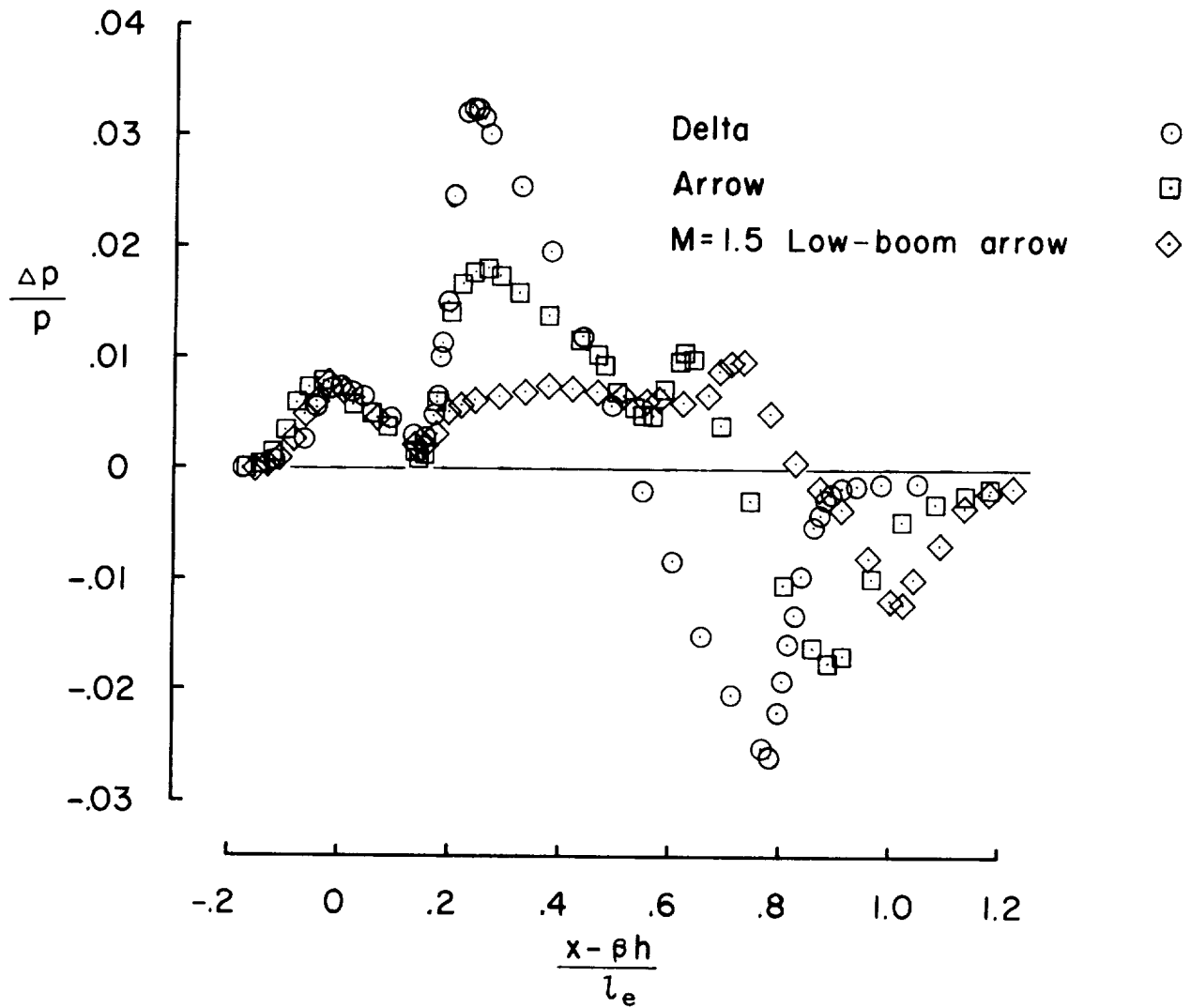
(d) Reference models and Mach 1.5 low-boom arrow-wing model.

Figure 12.- Concluded.
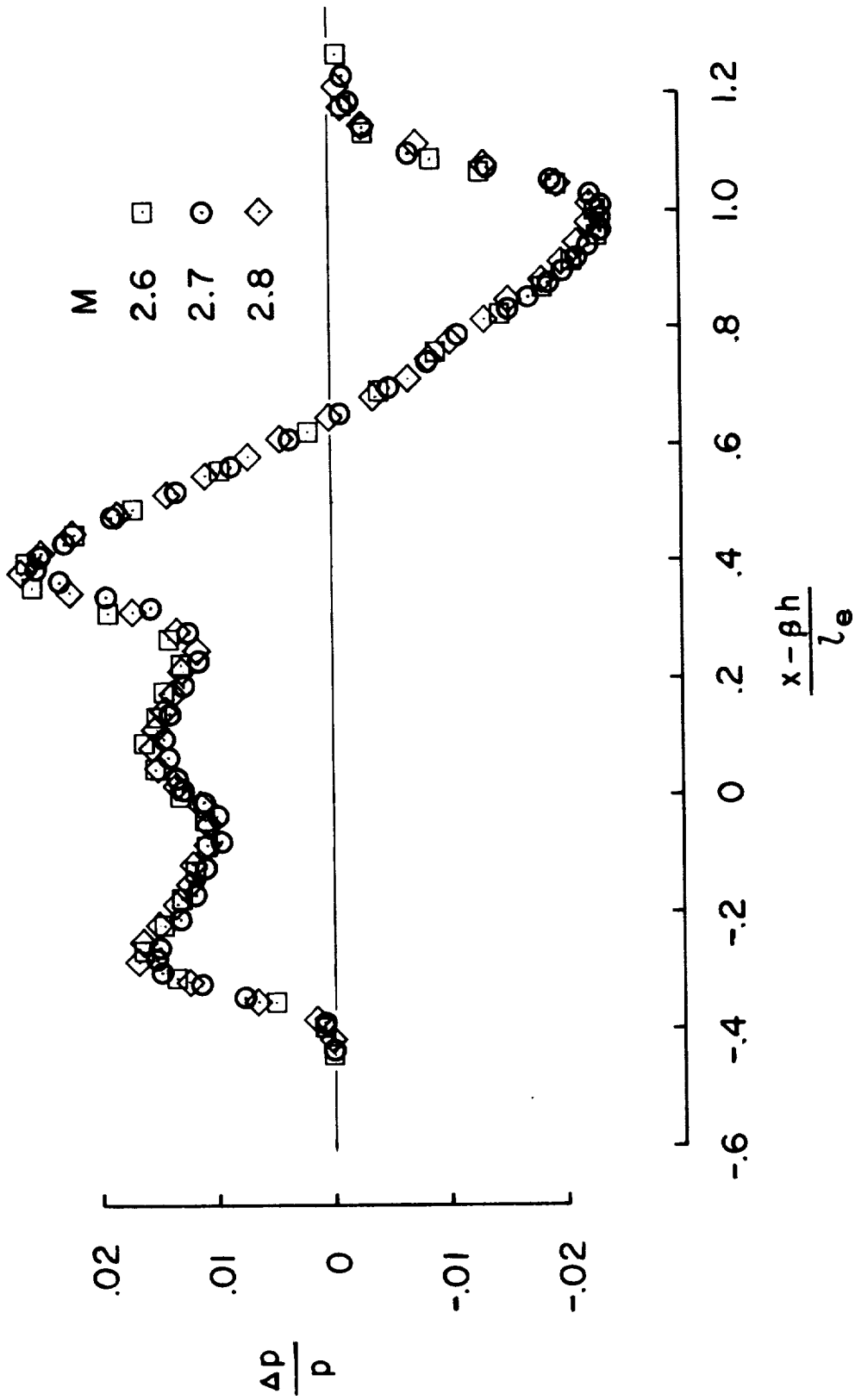
(a) $\alpha = \alpha_D$ with $M = 2.6$, 2.7, and 2.8.
Mach 2.7 low-boom arrow-wing model.

Figure 13.- Measured pressure signature sensitivity with Mach number and angle of attack.

(b) M = 2.7 with $\alpha/\alpha_D = 0.8$, 1.0, and 1.2.

Figure 13.- Concluded.

Theory(inviscid) — — — — —

Theory(inviscid, boom-constrained) ——— — ———
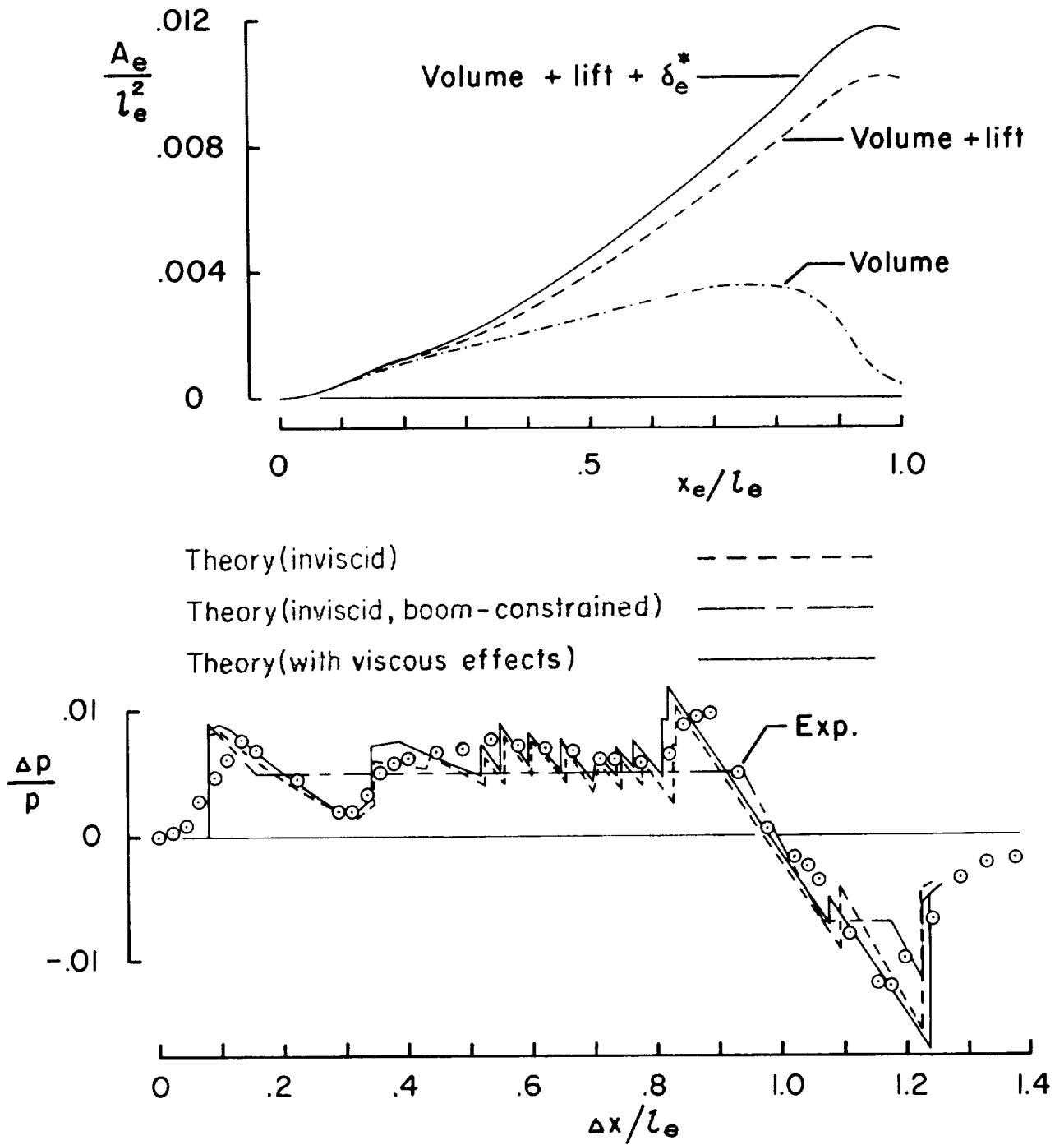
Theory(with viscous effects) —————
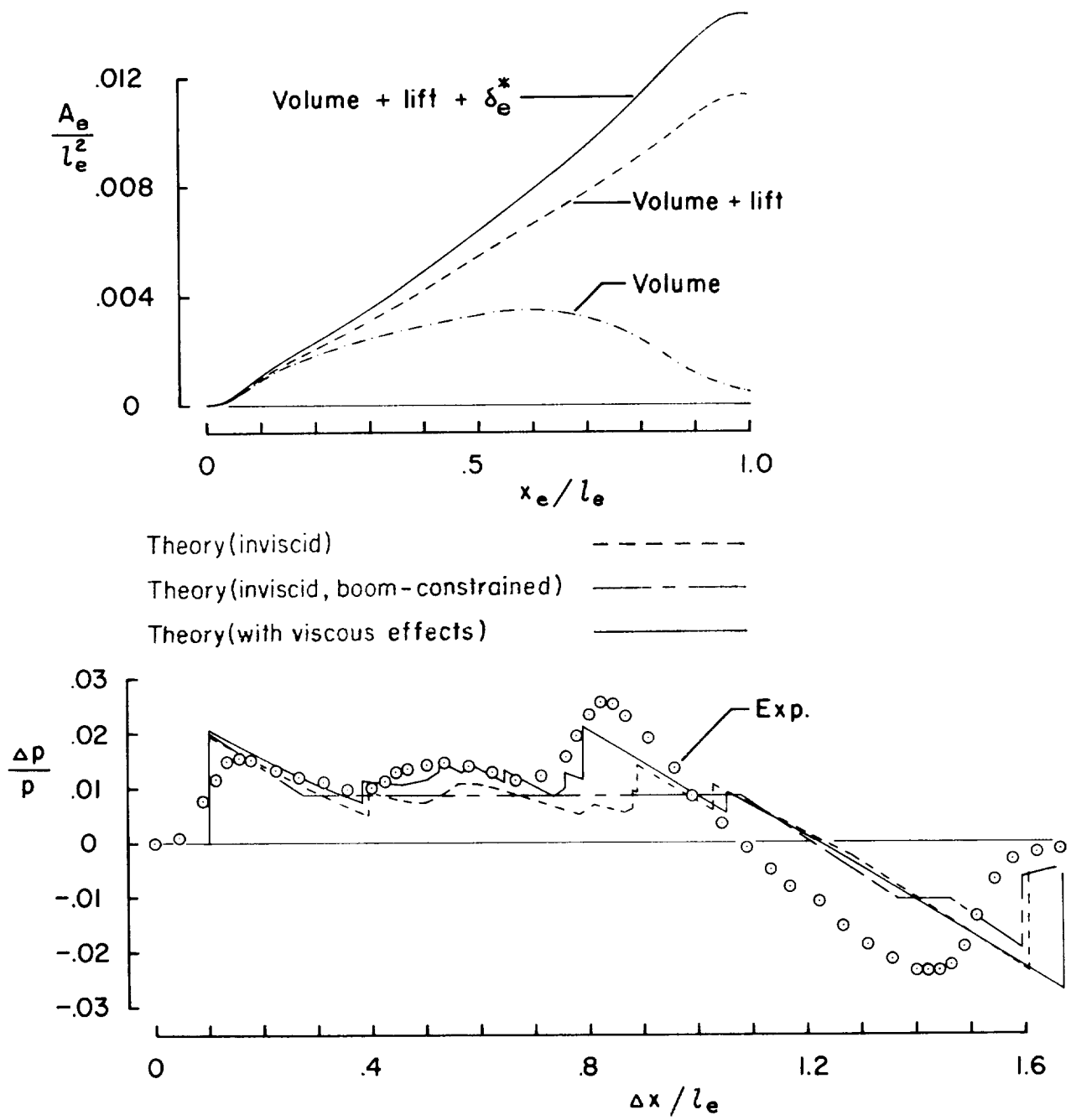
(a) Mach 2.7 low-boom arrow-wing model.

Figure 14.- Comparison of theory and experiment at M_D, $h/l_e = 3$, and $\alpha/\alpha_D = 1.0$.
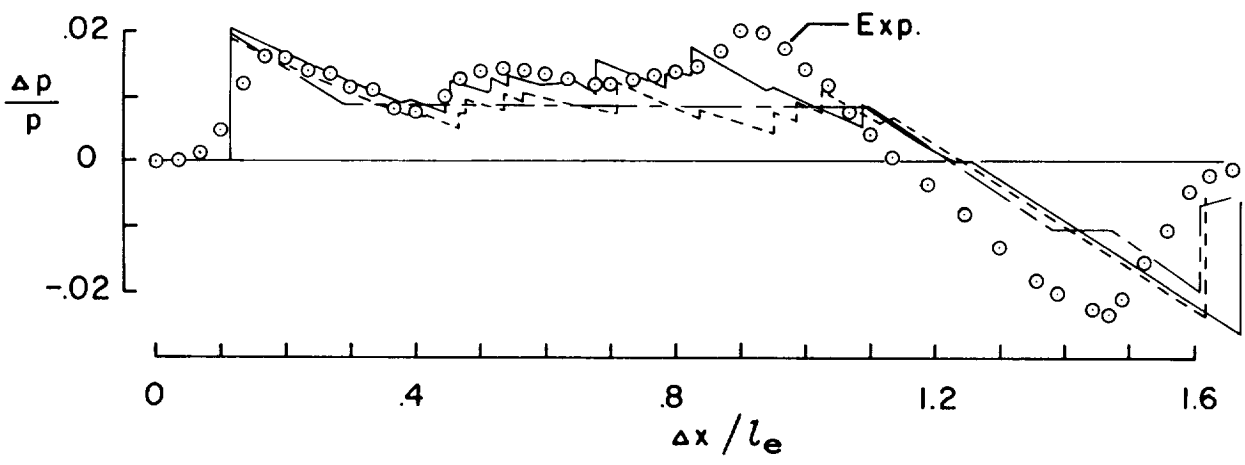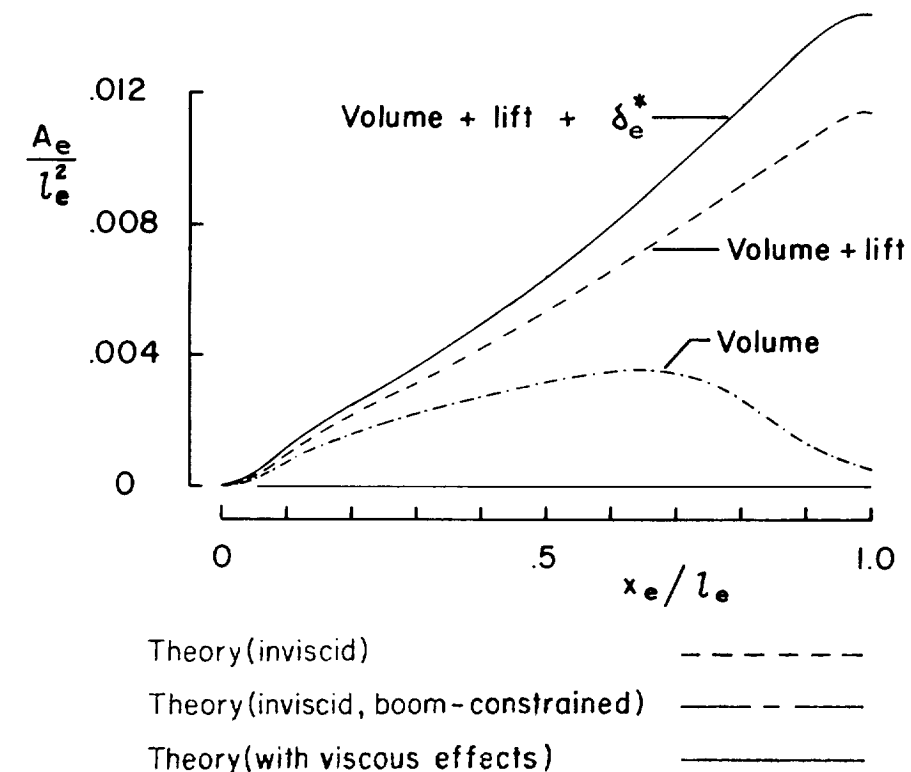
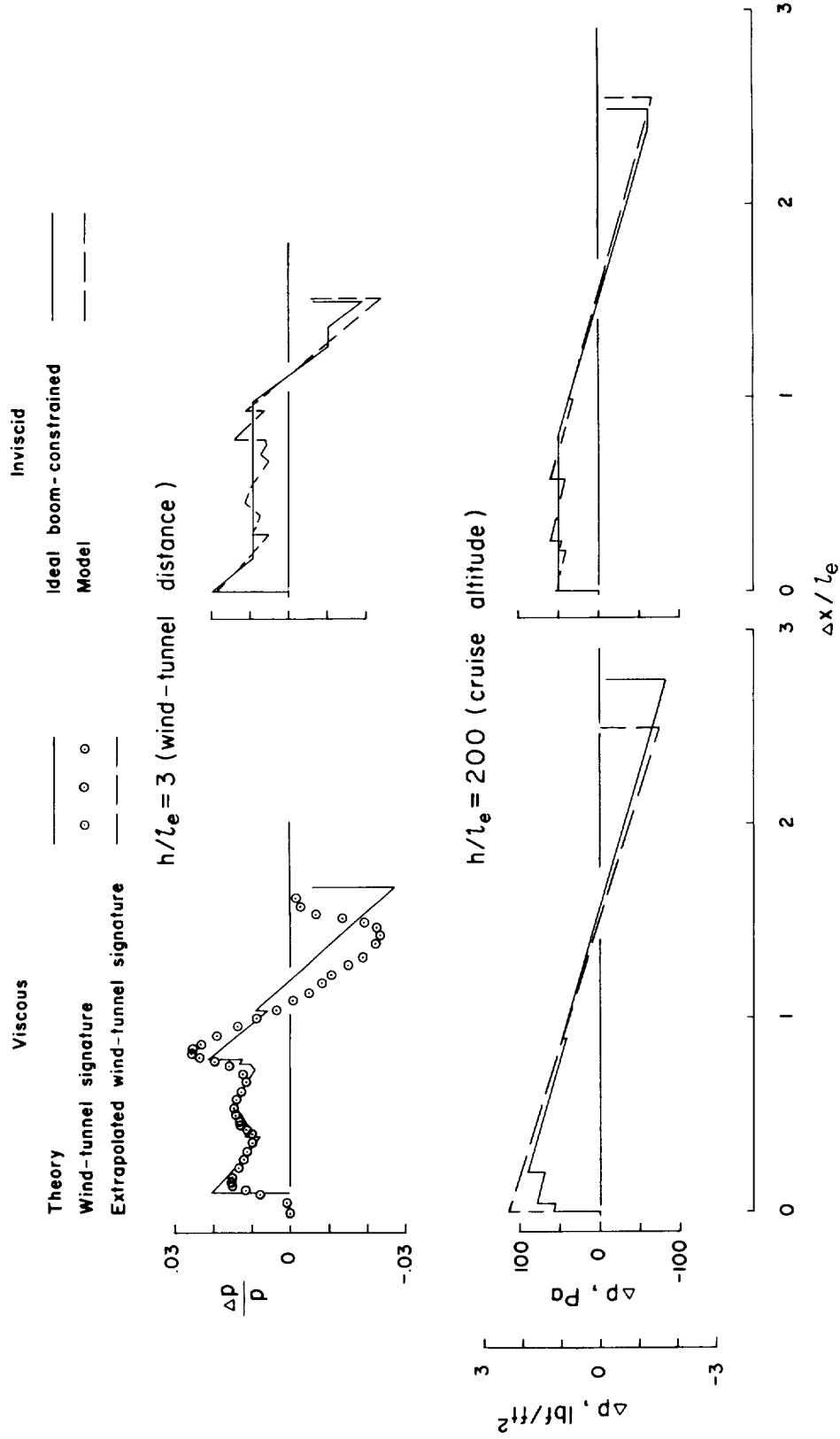(b) Mach 2.7 blunted arrow-wing model.

Figure 14.- Continued.

$\dfrac{A_e}{l_e^2}$

.012

.008

.004

0

Volume + lift + δ_e^*

Volume + lift

Volume

0   .5   1.0

x_e/l_e

Theory (inviscid) — — — —

Theory (inviscid, boom-constrained) — — —

Theory (with viscous effects) ————

$\dfrac{\Delta p}{p}$

.01

0

-.01

Exp.

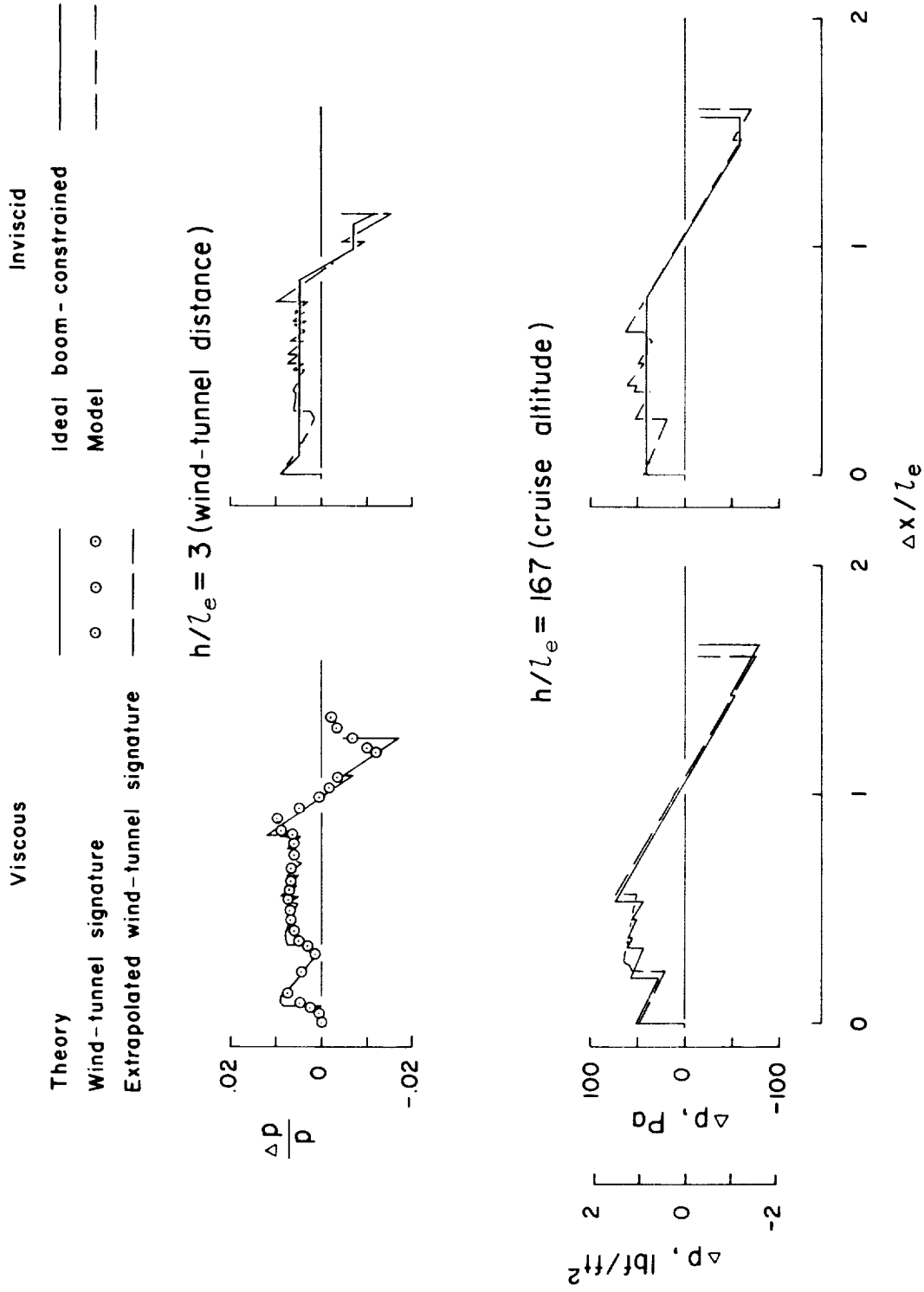0   .2   .4   .6   .8   1.0   1.2   1.4

$\Delta x/l_e$

(c) Mach 1.5 low-boom arrow-wing model.

Figure 14.- Concluded.

(a) Mach 2.7 low-boom arrow-wing model. $M = 2.7$; $\alpha/\alpha_D = 1.0$; $h = 18\ 288$ m (60 000 ft); $K_r = 1.9$.

Figure 15.— Comparison of extrapolated signatures with and without boundary-layer effects.

43

Figure 15.- Concluded.

(b) Mach 1.5 low-boom arrow-wing model. $M = 1.5$; $\alpha/\alpha_D = 1.0$; $h = 15\ 240$ m (50 000 ft); $K_r = 1.9$.

44

1. Report No. NASA TP-1421	2. Government Accession No.	3. Recipient's Catalog No.
4. Title and Subtitle WIND-TUNNEL INVESTIGATION OF THE VALIDITY OF A SONIC-BOOM-MINIMIZATION CONCEPT		5. Report Date October 1979
		6. Performing Organization Code
7. Author(s) Robert J. Mack and Christine M. Darden		8. Performing Organization Report No. L-12661
		10. Work Unit No. 517-53-43-03
9. Performing Organization Name and Address NASA Langley Research Center Hampton, VA 23665		
		11. Contract or Grant No.
		13. Type of Report and Period Covered Technical Paper
12. Sponsoring Agency Name and Address National Aeronautics and Space Administration Washington, DC 20546		
		14. Sponsoring Agency Code

15. Supplementary Notes

16. Abstract

A wind-tunnel investigation has been conducted to determine the validity of a sonic-boom-minimization theory. Five models - two reference and three low-boom constrained - were tested at design Mach numbers of 1.5 and 2.7. Results showed that the pressure signatures generated by the low-boom models had significantly lower overpressure levels than those produced by the reference models and that small changes in the Mach number and/or the lift caused relatively small changes in the signature shape and overpressure level. Boundary-layer effects were found to be sizable on the low-boom models, and when viscous corrections were included in the analysis, improved agreement between the predicted and the measured signatures was noted. Since this agreement was better at Mach 1.5 than at Mach 2.7, it was concluded that the minimization method was definitely valid at Mach 1.5 and was probably valid at Mach 2.7, with further work needed to resolve the uncertainty.

17. Key Words (Suggested by Author(s)) Sonic boom Minimization theory Experimental study	18. Distribution Statement Unclassified - Unlimited Subject Category 02

19. Security Classif. (of this report) Unclassified	20. Security Classif. (of this page) Unclassified	21. No. of Pages 44	22. Price* $4.50